Prospectivity analysis of orogenic gold deposits in Saqez-Sardasht Goldfield, Zagros Orogen, Iran

Alireza Almasi, Mahyar Yousefi, Emmanuel John M. Carranza

PII: S0169-1368(17)30173-7
DOI: https://doi.org/10.1016/j.oregeorev.2017.11.001
Reference: OREGEO 2387

To appear in: *Ore Geology Reviews*

Received Date: 2 March 2017
Revised Date: 7 August 2017
Accepted Date: 4 November 2017

Please cite this article as: A. Almasi, M. Yousefi, E.J.M. Carranza, Prospectivity analysis of orogenic gold deposits in Saqez-Sardasht Goldfield, Zagros Orogen, Iran, *Ore Geology Reviews* (2017), doi: https://doi.org/10.1016/j.oregeorev.2017.11.001

Prospectivity analysis of orogenic gold deposits in Saqez-Sardasht Goldfield, Zagros Orogen, Iran

Alireza Almasi[1], Mahyar Yousefi✉[,2], Emmanuel John M. Carranza[3,4,5]

[1]*Young researchers and Elites club, Science and Research Branch, Islamic Azad University, Tehran, Iran*

[2]*Faculty of Engineering, Malayer University, Malayer, Iran*

[3]*Geological Sciences, School of Agricultural, Earth and Environmental Sciences, University of KwaZulu-Natal, South Africa*

[4]*Economic Geology Research Centre (EGRU), James Cook University, Queensland, Australia*

[5]*Institute of Geosciences, State University of Campinas (UNICAMP), Campinas, São Paulo, Brazil*

Abstract

Diverse deposit-types or mineral systems form by diverse geological processes, so translation of knowledge about the controls of mineralization acquired from the 4D geological modeling into 2D spatial predictor maps is a major challenge for prospectivity analysis. In this regard, mathematical functions have been used to model the conceptual or perceived spatial relationships between geological variables and targeted type or system of mineralization. In this paper, due to the different models of spatial relationships between predictors and mineral deposits, we investigated the performance of different fuzzification functions to quantify the relationships. We demonstrated that various types of relationships between exploration features and a mineralization-type sought could be quantified using different fuzzification functions for prospectivity analysis. We illustrated the process of the prospectivity analysis by using a data set of orogenic gold deposits in Saqez-Sardasht Goldfield, Iran. Prospectivity modeling of orogenic gold mineralization in the study area showed that the NE-SW trending targets have priority for further prospecting of the deposits.

Keywords: Spatial relationship; Mineral deposits; Prospectivity analysis; Zagros Orogen; Iran; Orogenic Gold.

✉ Corresponding author: Malayer University, Malayer, Iran. Tel.: +98.911.3385443. Postal Code: 65719-95863. E-mail address: M.Yousefi.Eng@gmail.com.

1. Introduction

For mineral prospectivity mapping (MPM) of a deposit-type sought in an area, mathematical functions have been used to model spatial relationships between geological variables system of mineralization (e.g., Bonham-Carter, 1994; Luo and Dimitrakopoulos, 2003; Porwal et al., 2003a,b,c; Carranza, 2008, 2017). In MPM, mathematical functions, have been widely used to assign weights to discretized spatial evidence values as fuzzified evidential maps in the [0,1] range or to rank target areas as fuzzy prospectivity models (e.g., Bonham-Carter, 1994; Carranza and Hale, 2002; Luo and Dimitrakopoulos, 2003; Porwal et al., 2003c; Carranza, 2008, 2009, 2017; Lisitsin et al., 2013; Mutele et al., 2017; Nykänen et al., 2017). The weights assigned to classes of discretized evidential values may be based on (a) expert judgment directly, (b) locations of known mineral occurrences (KMOs), (c) a combination of (a) and (b), or (d) subjectively-defined functions, so indirectly-assigned by analyst (e.g., Luo, 1990; Bonham-Carter, 1994; Cheng and Agterberg, 1999; Luo and Dimitrakopoulos, 2003; Porwal et al., 2003a,b,c, 2004, 2006; Carranza et al., 2005; Carranza, 2008, 2014; Porwal and Kreuzer, 2010; Mejía-Herrera et al., 2014; Carranza and Laborte, 2016; McKay and Harris, 2016). All these methods impart bias due to discretization of continuous spatial values, use of subjective expert judgments, and sparse or incomplete data on locations of KMOs in knowledge- and data-driven MPM (Coolbaugh et al., 2007; Lusty et al., 2012; Ford et al., 2016).

To reduce bias in the assignment of weights to continuous-value spatial evidence, various researchers (e.g., Nykänen et al., 2008a; Yousefi et al., 2012, 2013, 2014; Yousefi and Carranza, 2015a, b, c, 2016a; Yousefi and Nykänen, 2016) have applied logistic functions to assign fuzzy weights to indicator features without using locations of KMOs and without discretization of evidential values into some arbitrary classes based on expert opinion. While this practice overcomes imprecise evaluation of the relative importance of evidential values, as portrayed by simplification and discretization of continuous-value evidential data into some arbitrary classes, it is also subjective because using a single logistic function for weighting spatial evidence values does not consider the fact that diverse deposit-types or mineral systems form by diverse geological processes. Thus, the spatial relationships of deposits with different predictors are variable. Consequently, selection of a suitable function is crucial in modeling the relative importance of every evidential map derived from particular spatial data sets. Furthermore, there are different models of spatial relationships between predictors and deposits, and thus, the assignment of weights to spatial evidence values is a highly critical exercise (Carranza, 2008). Joly et al. (2012) mentioned that the major challenge in GIS-based MPM is to translate the knowledge about the controls of mineralization acquired from 4D geological modeling into 2D-weighted spatial predictor maps. McCuaig et al. (2010) pointed out that there are challenging issues for linking scientific understanding of mineral systems to their translation in exploration evidence layers for MPM. Thus, eliciting mineralization-related geological and exploration features, representing the deposit-type or mineral system of interest in a study area is a challenge as well (e.g., Asadi et al., 2015).

To address the above-mentioned challenges in this paper, we first examined mineralization system of the deposit-type sought to elicit exploration indicator features. Then, we trialed different types of logistic functions, namely large, small, and near, that were proposed by Tsoukalas and Uhrig (1997) and applied by Yousefi and Carranza (2015a,b,c, 2016b) and Yousefi and Nykänen (2016), in order to quantify diverse relationships between spatial evidence values and the deposit-type sought. We tested different types of logistic functions because, as McCuaig et al. (2010) pointed out, the mineral system approach needs to be adapted in different areas with various geological setting for translating mineralization-related processes to MPM. To illustrate the process of eliciting exploration indicator features and the application of the proposed functions, to demonstrate their ability in weighting different types of spatial evidence values, and to test the methodology, we selected a suitable area in the Kordestan province in northwest Iran where suitable data are available to analyze prospectivity for orogenic gold deposits.

2. The study area and regional geological background

The study area is situated in the Zagros orogenic belt of Iran (Fig. 1a). This belt, as part of the Alpine-Himalayan mountain chain, extends for about 2000 km in a NW–SE direction from the East Anatolian fault of eastern Turkey to the Oman Line in southern Iran (Alavi, 1994). The subduction of the Neo-Tethyan ocean floor beneath Iran sutured Iran to Arabia (e.g. Takin, 1972; Berberian and King, 1981; Alavi, 1980, 1994), and the subsequent continental convergence built the Zagros Orogenic Belt (e.g., Ghasemi and Talbot, 2006). This belt consists of three tectonically related parallel zones, which are, from northeast to southwest (Fig. 1a) (Alavi, 1994): (1) the Urumieh–Dokhtar Magmatic Assemblage (UDMA); (2) the Sanandaj–Sirjan Zone (SSZ); and (3) the Zagros Simply Folded Belt.

The SSZ has a width of 150–250 km and lies to the southwest of the UDMA (Stocklin, 1968). The rocks in the SSZ are highly deformed and share the NW–SE trend of its structures (Ghasemi and Talbot, 2006). The rocks in the SSZ are mostly of Mesozoic age with Paleozoic rocks rarely exposed except in the southeast where they are predominant (Berberian and King, 1981). The SSZ is characterized by metamorphic and deformed rocks, which associated with abundant deformed and undeformed plutons, and presence of widespread Mesozoic volcanic rocks (Mohajjel et al., 2003). During and after the Middle Triassic phase of activity, andesitic-basaltic volcanism and acid granitic intrusions formed along the SSZ (Berberian and King, 1981). The SSZ can be subdivided into two parts (Eftekharnejad, 1981) (Fig. 1a): (1) the southern part (south SSZ) consists of rocks deformed and metamorphosed in Middle to Late Triassic; and (2) the northern part (north SSZ), deformed in the Late Cretaceous, contains many intrusive felsic rocks (Ghasemi and Talbot, 2006).

The study area in this paper measures ~2,000 km^2 and is located in the Saqez-Sardasht orogenic goldfield in the north SSZ, northwest Iran (Fig. 1b). The area is covered by the 1:100,000 scale Saqez quadrangle map (Fig. 1c) prepared by the Geological Survey of Iran (GSI) (Babakhani et al., 2003).

3. Deposit model and data used

3.1. General characteristics of orogenic gold deposits

Orogenic gold deposits are a widespread coherent group of epigenetic mineral deposits controlled by a similar set of factors (Groves, 1993; Knox-Robinson, 2000) and are sited in accretionary or collisional orogens of all ages. Orogenic lode-gold deposits formed from deep-seated hydrothermal fluids with Au transported as thio-complexes (Groves et al., 2000). These deposits are hosted in Precambrian greenstone belts and Precambrian–Phanerozoic accretionary sedimentary belts, and commonly show predictable and repetitive structural geometries (Groves et al., 2000). They evolved along the southern Gondwana margin and the northern side of the Paleo-Tethys Ocean during the Paleozoic, and within the circum-Pacific accreted terranes in the Mesozoic–Tertiary (Goldfarb and Groves, 2015).

Structures are the first-order control on the formation and distribution of orogenic gold deposits, as high ore-fluid flux into permeable structures or fractured rock bodies is an essential ore control (Groves et al., 2000; Herbert et al., 2014; Carranza et al., 2015). Therefore, orogenic gold deposits display spatial relationships with fault corridors, shear zones, and crustal discontinuities that likely controlled flow of deep-seated hydrothermal fluids towards higher crustal levels (e.g., Groves et al. 1998; Sillitoe, 2000; Betts and Lister, 2002; Haynes, 2002; Grauch et al., 2003; Beaudoin et al., 2006; Bierlein et al., 2006b; Almasi et al., 2014).

Geological settings of orogenic gold deposits are extremely complex, which resulted in highly variable host rocks (Goldfarb et al., 2001; Goldfarb and Groves, 2015). Gold mineralization is dominantly hosted by metagreywackes, metavolcanic, metasedimentary and metamorphic rocks of a variety of geological ages (Bark and Weihed, 2012; Groves et al., 2000; Fu et al., 2012). Lithological contacts separating rocks of strongly contrasting rheologies are important to measure the relationship between geological structures, lithological boundaries and gold mineralization (Groves et al., 2000; Herbert et al., 2014).

There are clear close geometrical and temporal relations between intrusions and gold emplacement structures (Craw et al., 2006). The fundamental driver for orogenic gold systems is high fluid flux that requires an effective thermal engine (Bierlein et al., 2006a). Mafic, ultramafic, and granitoids intrusions are spatially and temporally associated with gold mineralization (Bierlein et al., 2006a; Bark and Weihed, 2012; Joly et al., 2012; Knox-Robinson, 2000; Fu et al., 2012).

In regard of the foregoing discussion, two main types of orogens have been recognized – internal orogens (i.e., collisional orogens for example Variscan, Appalachian and Alpine orogens) and external orogens (i.e., accretionary orogens for example the American Cordillera) (Murphy and Nance, 1992; Bark and Weihed, 2012). Internal orogens are commonly considered less permissive for orogenic gold formation and this orogen should be considered relatively weakly mineralized due to its internal-type, unmineralized nature (Bark and Weihed, 2012). However, in some orogenic gold mineral systems, in particular in the Birimian gold mineral systems of West Africa, granitoids are

often mineralized. The explanation for that is that deformation causes the less competent metasedimentary country rocks to fail by shearing, but given that these rocks are very tight due to previous shortening and deformation no, or only very little, new space is created. The granitoid bodies, on the other hand, fail by fracturing creating low stress sites and space for gold deposition. The fracturing event triggers increased permeability and suction and thus focuses fluid flow into the newly created facture network / stockwork, centered upon granitoid intrusions.

Orogenic-gold deposits are associated with indicative geochemical anomalies, which have been widely used as a reconnaissance-scale exploration tool (Nykänen, 2008; Nykänen et al., 2008a,b; Nykänen and Salmirinne, 2007; Bierlein and McKnight, 2005; Fu et al., 2012; Groves et al., 2000; Goldfarb et al., 2001; Carranza et al., 2015).

In this study, to apply knowledge of critical processes of mineralization in an orogenic gold system to prospectivity analysis (e.g., Groves et al., 2000; McCuaig et al., 2010; Lisitsin et al., 2010; Herbert et al., 2014; Carranza et al., 2015; Asadi et al., 2016; Duarte Campos, 2017), district-scale mapping of prospectivity for the deposit-type sought was considered appropriate to delineate target areas for further exploration at camp-scale. Following the discussion in Carranza et al. (2015), district-scale of mapping was selected considering the sorts of data available in the study area (see next sub-section), which is covered by the 1:100,000 scale geological map (Fig. 1c) with respect to the general district-scale characteristics of system of orogenic gold mineralization summarized in Table 1.

3.2. Datasets

In recent years, the Saqez-Sardasht region has been surveyed for several types of mineral deposits because of its favorable geological settings (Aliyari et al., 2009, 2012; Tajeddin, 2011; Almasi et al., 2014, 2015a,b). The various exploration data sets gathered during those surveys are available and have been used for the analyses in this paper. Geochemical data pertain to 535 stream sediment samples, gathered by GSI, which were chemically analyzed for Au using fire assay method and for As, Bi and Hg by inductively coupled plasma mass spectrometry. Analytical detection limits were 1 ppb for Au, 0.5 ppm for As, and 0.1 ppm for Bi and Hg. The method of Thompson and Howarth (1976) was applied for assessing the analytical precision using duplicated samples. The precision was better than 10% for the selected elements.

Magnetic and radiometric data, obtained from helicopter-borne geophysical surveys conducted in the north and south parts of the area. In the north part with area of ~1767 km^2, the data were gathered by Atomic Energy Organization of Iran in 1976 with a line spacing and flight elevation of 500 and 120 meters, respectively. In the south part with an area of ~ 283 km^2, the geophysical surveys were conducted by Fugro Airborne Surveys Corporation and GSI in 2006 with a line spacing and flight elevation of 200 and 60 meters, respectively. These geophysical data were interpreted individually, and were interpolated using minimum curvature method (e.g., Akima, 1970; Smith and Wessel, 1990) and the same grid cell size of 100 m × 100 m, just as the other evidence layers. It is notable that only

seven percent of the study area is covered, so the area is suited for radiometric surveys.

3.3. Conceptual model of orogenic gold deposits and exploration criteria in the study area

The study area, which is located in the Saqez-Sardasht orogenic gold zone, a ductile to brittle shear zone (Aliyari et al., 2007, 2009), comprises a regional E–W trending gold belt with seven known gold occurrences (Fig. 1b) hosted by upper Cretaceous to Tertiary mafic to intermediate metavolcanic and metasedimentary rocks (Table 2). Figure 2 shows the Au-bearing rocks in the gold occurrences. The structural studies on the gold deposits/occurrences revealed that all of them are hosted in ductile to brittle shear zone. The gold occurrences are spatially associated within, or adjacent to, the major deep Saqez-Sardasht thrust fault (Fig. 1b) with ~100 km in length (Aliyari et al., 2012) and the normal fault systems across this structural zone (Mohajjel et al., 2003; Aliyari et al., 2009, 2012; Tajeddin, 2011).

Based on previous geochemical and stable isotope investigations (Aliyari et al., 2009, 2012; Tajeddin, 2011), the genesis of the gold deposits in the study area likely involved metamorphic devolatilization and dehydration processes that firstly leached Au from deeper parts of Fe-rich mafic and meta-volcanic rocks. The gold veins and veinlets were then deposited in the upper metamorphosed mafic to felsic volcanic and sedimentary rocks (e.g., greenschist facies). The granitoids played an important "heat engine" role, activating the percolation of gold-bearing fluids (Aliyari, 2006; Aliyari et al., 2007, 2009, 2012). Mineralogical studies revealed that oxide minerals in mafic meta-volcanic rocks are generally magnetite, titanomagnetite and ilmenite, which make them detectable using aeromagnetic data (Aliyari, 2006). Additionally, mylonitic granites and altered mylonitic granites, which were indicated as a secondary host rocks, have relatively higher radioactive-elements content in their minerals (feldspar, plagioclase, zircon: Aliyari, 2006; Tajeddin, 2011) than other rock units of the study area and can be detected using airborne geophysical survey. Furthermore, because the geological units have various magnetic characteristics, contacts and discontinuities between these units can be identified efficiently using edge detection methods (Airo, 2001, 2007; Bierlein et al., 2006a,b; Henson et al., 2010; Ferreira et al., 2011; Almasi et al., 2014).

Based on the characteristics of orogenic gold deposits in well-explored areas as well as in the study area of this paper, the localization of orogenic gold deposits within an endowed geological setting requires the synthesis of several critical factors, which can be defined in terms of a minerals system. These factors are (e.g., Groves et al., 2000; Bierlein et al., 2006a; Aliyari et al., 2009, 2012; Tajeddin, 2011; Carranza et al., 2015): (1) metal source(s); (2) superior structural plumbing systems, such as fault, geological contact, and shear zones; and (3) ore trap such as reactive host rocks.

To translate the above-mentioned conceptual model of the deposit and the critical factors controlling the gold mineralization in the study area into spatial predictor maps to be used in the GIS-based MPM, and based on the available spatial datasets, we generated five individual maps of evidence of prospectivity for orogenic-Au deposits. These maps are: (i) proximity to granitoids (e.g., Groves et al., 2000; Knox-Robinson, 2000; Nykänen et al., 2008a,b; Bark and Weihed, 2012; Herbert

et al., 2014) as "heat engine" evidence layer, representing activation of the percolation of fluids; (ii) structural evidence layer representing corridors and crustal discontinuities that controlled pathways of deep-seated hydrothermal fluids into higher crustal levels (e.g., Groves et al., 2000); (iii) map of K/Th ratio as evidence of hydrothermal activities (e.g., Ario, 2002, 2007; De Quadros et al., 2003; Almasi et al., 2015a) representing active pathways; (iv) proximity to metasedimentary and metavolcanic rocks as a proxy for regional rheology contrast (cf. Nykänen et al., 2008a,b; Groves et al., 2000; Joly et al., 2012; Herbert et al., 2014) representing trapping mechanism; and (iv) multi-element geochemical signature modeled as geochemical mineralization prospectivity index (GMPI) as indicator of the deposit-type sought (Yousefi et al., 2012, 2014) representing metal deposition.

The 1:100,000 scale geological map of Saqez (Fig. 1c), prepared/published by the GSI (Babakhani et al., 2003), was used to generate heat engine and ore trap evidence layers. The geophysical data were used to generate two evidence layers, namely: (a) structural evidence layer and (b) evidence layer of hydrothermal activities. Each of the evidence maps was generated by using a suitable logistic function (Tsoukalas and Uhrig, 1997; Nykänen et al., 2008a,b; Yousefi et al., 2012, 2013, 2014; and Yousefi and Carranza, 2015a,b) modeling the relationship of mineral deposits and the spatial evidence values (see section 4.1 below). For deposition of orogenic gold, source rock is required from which available gold can be leached and transported effectively to the site of deposition (e.g. Bierlein et al., 2006a). In the study area, plausible sources of Au are the deeper parts of Fe-rich mafic and metavolcanic rocks (Aliyari et al. 2009).

4. Methods

Translation of mineral systems into weighted evidential layers is a challenge for MPM (McCuaig et al., 2010) and requires understanding of relationships between evidential features and mineral deposit-type sought (Carranza, 2008). In this paper, geochemical, geophysical-potential and proximity data were used to derive district-scale spatial proxies for processes critical to orogenic-Au systems, which were then transformed into fuzzy evidential layers using appropriate logistic functions resulting in evidential values in the range [0,1]. The selection of appropriate logistic function is based on the spatial relationship of continuous evidence values and mineral deposits of the type sought. The fuzzy values are taken as weights. After generation of fuzzy evidence layers, each of which represents a certain exploration criterion of prospectivity for orogenic-Au deposits or a critical process of orogenic-Au systems, they were integrated to model orogenic-Au prospectivity.

4.1. Fuzzification functions

Transformation of data (e.g., binarization, multi-class representation, continuous-value) provides a set of values with more discriminatory information and less redundancy for classification (Micheli-Tzanakou, 1999). Defining a suitable non-linear transformation into a new space could facilitate interpretation of a pattern for a set of evidential values in MPM compared to their original space (Bishop, 2006; Yousefi et al., 2014; Yousefi and Carranza, 2015b). A logistic transformation has

played an important role in many classification algorithms and pattern recognition (Bishop, 2006), such as statistics, neural networks, machine learning, and expert systems (e.g., Micheli-Tzanakou, 1999; Berthold and Hand, 2002; Alpaydm, 2004; Fink, 2007). Recently, Yousefi et al. (2014) and Yousefi and Carranza (2015b) compared linear and non-linear transformations of evidential data using logistic function and demonstrated that the latter is much better for weighting of evidential data in fuzzy MPM. A logistic function maps the map data space into the [0,1] range. There is a family of logistic functions (Tsoukalas and Uhrig, 1997; Theodoridis and Koutroumbas, 2006) that can be used to transform data into logistic space based on minimum and maximum values and slope variations between them. Accordingly, different but suitable logistic functions have been used for transforming evidential values into the [0,1] range to support fuzzy logic MPM (Carranza and Hale, 2002; Carranza, 2008; Theodoridis and Koutroumbas, 2006; Yousefi et al., 2012, 2013, 2014; Mutele et al., 2017; Nykänen et al., 2017). Unbounded spatial evidence values can properly be transformed into in the [0,1] range using a logistic function (e.g., Bishop, 2006). As Nykänen et al. (2008a), Yousefi et al. (2012, 2013, 2014), Yousefi and Carranza (2015a,b,c), and Yousefi and Nykänen (2016) demonstrated, evidential maps with spatially continuous weights can be generated by application of a logistic function without using locations of known mineral occurrences and without discretization of evidential values into some arbitrary classes. Yousefi and Carranza (2015a) used Eq. (1), a logistic sigmoid (S shape) function, to weight continuous-value spatial evidence:

$$\mu_x = \frac{1}{1+e^{-s(x-i)}} \tag{1}$$

where μ_x is a score in the [0,1] range, fuzzy weight in logistic space, i and s are inflexion point and slope, respectively, of the logistic function, and X is evidential value of each pixel in an input map (e.g., values of geochemical signatures and the value of proximity to geological features) for which μ_x is estimated. The parameters i and s determine the shape of the logistic function and, hence, the output fuzzy weights. Yousefi and Nykänen (2016) assigned the values of 0.01 and 0.99, respectively for the lowest and the highest spatial evidence values, X_{min} and X_{max}, to obtain two equations in a system. Then by solving the system of equations, i and s were determined based on the X_{min} and X_{max} as Eq. [2] and Eq. [3]:

$$s = \frac{9.2}{X_{max} - X_{min}} \tag{2}$$

$$i = \frac{X_{max} + X_{min}}{2} \tag{3}$$

Therefore, the application of Eq. (1) results in highest and lowest fuzzy scores, i.e., 0.99 and 0.01, respectively, for the maximum and minimum values of spatial evidence. Variations of fuzzy score of

spatial evidence using different *i* and *s* values were pointed out by Yousefi and Nykänen (2016). Likewise, in this paper, to transform unbounded spatial evidence values into the [0, 1] range, we used various types of logistic function namely Small, Large, and Near (Masters, 1993; Zadeh, 1993; Tsoukalas and Uhrig, 1997; Burrough and McDonnell, 1998; Kemp et al., 2001; Nykanen et al., 2008a,b; Almasi et al., 2015a,b; Yousefi and Carranza, 2015a,b,c; Yousefi and Nykänen, 2016).

4.1.1 Small fuzzification function

There are situations where low evidence values have strong spatial association with mineral deposits. For example, mineral deposits typically exist in close proximity (i.e., short distances) to certain geological features. In such situations, low evidence values must be represented by high scores (weights) whereas high evidence values low scores. Such situations should be modeled with a small fuzzification function, which has the following form (Tsoukalas and Uhrig, 1997):

$$\mu_X = \frac{1}{1 + (\frac{X}{f_2})^{f_1}} \tag{4}$$

where X is spatial evidence value, μ_X is a score in the [0,1] range corresponding to X, fuzzy weight in logistic space, f_1 is the spread of the transition from a membership value of 1 to 0, and f_2 is the midpoint in the data set of evidence values where the fuzzy membership value is assigned by a score of 0.5.

4.1.2 Large fuzzification function

In other situations, high evidence values have strong spatial association with mineral deposits. For example, mineral deposits typically have spatial correlation with high values of geochemical anomalies. In such situations, high evidence values must be given high scores whereas low evidence values low scores. Such situations must be modeled with a large fuzzification function, which has the following form (Tsoukalas and Uhrig, 1997):

$$\mu_X = \frac{1}{1 + (\frac{X}{f_2})^{-f_1}} \tag{5}$$

where X is spatial evidence value, μ_X is a score in the [0,1] range corresponding to X, fuzzy weight in logistic space, f_1 is the spread of the transition from a membership value of 1 to 0 and f_2 is the midpoint in the data set of evidence values where the fuzzy membership value is assigned by a score of 0.5.

4.1.3 Near fuzzification function

There are situations where mineral deposits have strong spatial associations with intermediate evidence values but not with lowest and highest evidence values. For example, in some geological settings mineral deposits occurred where aeromagnetic data have intermediate values resulting from low magnetic intensity of argillic alteration and high magnetic intensity of iron ores. In such situations, intermediate evidence values must be given highest scores whereas the lowest and highest evidence values lowest scores. Such situations must be modeled using a near fuzzification function, also known as a sinusoidal membership function, which has the following form (Burrough and McDonnell, 1998; Tsoukalas and Uhrig, 1997).

$$\mu_X = \frac{1}{1 + (f_1 * (X - f_2))^2} \tag{6}$$

where X is spatial evidence value, μ_X is a score in the [0,1] range corresponding to X, fuzzy weight in logistic space, f_1 is the spread of the transition from a membership value of 1 to 0 and f_2 is the midpoint where the membership value is 1.

In the Equations (4), (5), and (6), the spread and mid parameters of the function can be defined subjectively to reflect the expert opinion or they can be defined objectively using solving a system of equations (Yousefi and Nykänen, 2016). Spread is a parameter of the fuzzification algorithm that determines how rapidly the fuzzy membership values decrease from 1 to 0, in fact, variations slope of the fuzzy score. Mid is intermediate evidence value in input dataset (the crisp value) that is given an intermediate score of 0.5 when using the small or large fuzzification functions, in fact, inflexion point, or that is given the highest score of 1, when using the near fuzzification function. Tsoukalas and Uhrig, (1997) have presented graphs showing the influence of different f_1 and f_2 values of small, large, and near functions in their corresponding output fuzzy memberships.

5. Results

5.1. Generation of weighted evidence layers

In the study area of this paper, there are only seven known gold occurrences, which were used to evaluate the models. All maps used in this paper were tessellated with a pixel size of 100 m × 100 m based on the density of geochemical sample point patterns (cf. Carranza, 2009; Hengl, 2006; Zuo, 2012). The following sub-sections describe the extraction and integration of proxies derived from mappable criteria, reflecting the district scale critical processes for orogenic gold formation.

5.1.1 Heat engine evidence layer

There is a common temporal and spatial relationship between granitoid rocks and orogenic gold deposits (Goldfarb et al., 2001; Groves et al., 2000; Fraser, 2002; Cross et al., 2005; Bark and

Weihed, 2012; Joly et al., 2012; Herbert et al., 2014) that is due to playing heat engine and metal source roles to the deposition of gold. Thus, the mineralization should occur in the proximity of the granite bodies, with the probability of a deposit being present decreasing with the increasing distance from the granites. Gold deposits near and around granitoids have been studied by Groves et al. (2000), Knox-Robinson (2000), Nykänen (2008), and Herbert et al. (2014). In the study area of this paper, there are granitoids of two periods (Aliyari, 2006; Aliyari et al., 2007, 2009 and 2012; Tajeddin, 2011): (1) granitoids, which were emplaced prior to the mineralization, causing an increase in the geothermal gradient and remobilization of large amounts of metamorphogenic fluids; and (2) granitoids that were emplaced earlier than the first group and were metamorphosed during the metamorphism processes (e.g., mylonitic granites). The later granitoids together with the meta-volcanic and meta-sedimentary rocks have been suggested as the ore traps. The former, unmetamorphosed, granitoids have been recognized as heat engine (cf. Aliyari et al., 2009, 2012; Tajeddin, 2011), thus Euclidian distance from these granitoids were calculated and fuzzified using small function (Eq. 4) representing heat engine evidence layer (Fig. 3a). Figure 3b represents how application of the small fuzzification function models the relative importance of low evidence values. Proximity to granitoids has been applied as spatial proxy of orogenic gold deposits in different areas (e.g., Nykänen, 2008; Joly et al., 2012).

5.1.2 Pathway evidence map

Gold deposits are strongly controlled by structures, e.g., faults, shears, thrusts, lithological contacts, and fold axes, (Groves et al., 2000; Knox-Robinson, 2000; Bierlein et al., 2006b; Joly et al., 2012; Herbert et al., 2014). Most mineralization is therefore expected to occur in the spatial proximity of these structures, and the closer an area is to structure, the higher the probability of finding a deposit in that area (Joly et al., 2012). Not only the structures control the location of gold deposits, they control the size of deposits: structure-proximal deposits tend to be larger (cf., Groves et al., 2000; Knox-Robinson, 2000; Joly et al., 2012). Due to the fact that not all of the structures may be active fluid pathways, distinguishing controlling structures is important (Bierlein et al., 2006b). Thus, interpretation of airborne geophysical data sets can be used to recognize parts of structures, which may subsequently be used as mineralization-related proxies representing the active fluid pathways (Groves et al., 2000; Nykänen et al., 2008b; Herbert et al., 2014).

Aeromagnetic data is known as an important source of information for studying lineaments and structures (Bierlein et al., 2006; Henson et al., 2010; Li, 2013; Almasi et al., 2014). In this study, after removing international geomagnetic reference field (IGRF), a reduction to magnetic pole (RTP: Baranov, 1957) filter was applied on the total magnetic intensity (TMI) data, in order to place the anomalies above their causative bodies. Then, to minimize the effects of shallow magnetic sources and to reduce noises associated with aeromagnetic data, upward continuation filter (UC) was applied. The edges of magnetic anomalies can represent lithological contacts, faults, fractures and crustal discontinuities (Bierlein et al., 2006; Henson et al., 2010), which are potentially controlling structures

for deposition of gold mineralization in the study area (Aliyari et al., 2007, 2009, 2012; Tajeddin, 2011; Almasi et al., 2014, 2015a,b). Thus, in order to detect the edges of aeromagnetic anomalies we applied total horizontal derivative (THD) filter (Airo, 2001, 2007; Bierlein et al., 2006a,b Henson et al., 2010; Ferreira et al., 2011; Almasi et al., 2014). The THD filter is used for multi-scale edge detection through aeromagnetic data (Archibald et al., 1999; Austin and Blenkinsop, 2008, 2009; Henson et al., 2010; Holden et al., 2000). Ferreira et al. (2011) proposed that applying tilt derivative (TDR) filter on the THD data facilitates the enhancement and visualization of magnetic edges. The TDR filter has been widely applied on aeromagnetic data for enhancement of magnetic edges and bodies (e.g., Ma and Li, 2012; Miller and Singh, 1994; Salem et al., 2007; Verduzco et al., 2004). Therefore, we used the TDR filter on THD data. As mentioned earlier in this paper, northern data were obtained from a higher flight elevation and wider line spacing in contrast with southern data, so have lesser resolution that would have introduced bias. Therefore, to modulate the bias resulting from the two surveys at different resolutions, the aforementioned interpretation processes were implemented separately on the north and south geophysical data. Then for further amending the bias, the values of TDR of the two data sets were individually transformed to the same space with the same minimum and maximum values, logistic space in [0, 1] range using large fuzzification function (Eq. 5). Finally, to generate fuzzy evidence layer of pathways (Fig. 4a) a mosaic of the two fuzzy sets were gridded and knitted together. Figure 4b shows how the application of large fuzzification function models the relative importance of spatial evidence values.

5.1.3 Evidence layer of hydrothermal activities

Airborne radiometric data are capable to map felsic igneous rocks, which contain high amounts of radioactive elements (i.e., Th, K and U) and the related hydrothermal activities (Silva et al., 2003; de Souza Filho et al., 2007; Magalhães and Souza Filho, 2012; Almasi et al., 2014). In this regard, the ratio of K/Th (after Airo, 2001, 2007) is used to recognize the above-mentioned geological features. Regions of K enrichment have been used to identify areas of hydrothermal alteration. However, it is difficult to separate elevated K values related to hydrothermal alteration from those related to lithology and weathering. To address this difficulty a well-known ratio of K/Th can be applied (e.g., Airo, 2001, 2007; Herbert et al., 2014; Almasi et al., 2015a). According to De Quadros et al., 2003, high values of K/Th ratios are good indicators for hydrothermally altered areas. In this paper, a fuzzy evidence layer of hydrothermal activities (Fig. 5a) was generated by transformation of K/Th values using large function (Eq. 5). Fig. 5b depicts how the application of large fuzzification function models the relative importance of K/Th ratios for prospecting gold mineralization.

5.1.4 Ore trap evidence map

The orogenic gold deposits are located in a multitude of different host rocks (Groves, 1993; Groves et al., 2000), for example meta-sedimentary and meta-volcanic rocks (shales, greenstones, amphibolite to granulite facies domains (Groves, 1993; Groves et al., 2000; Goldfarb et al., 2001; Fu et al., 2012; Herbert et al., 2014; Joly et al., 2012), which introduce problems for conceptually based

prospectivity mapping (Knox-Robinson, 2000). In the study area, these units consist of meta-volcano sedimentary units such as schists, amphibolites and mylonitic granites (Aliyari et al., 2007, 2009, 2012; Tajeddin, 2011) which have been portrayed in the geological map of the area (Fig. 1c). To transform the association of the orogenic gold deposits with meta-sedimentary and meta-volcanic rocks into an ore trap fuzzy evidence layer (Fig. 6a) for MPM, Euclidian distances from these units, were calculated and fuzzified using small function (Eq. 4). Fig.6b represents that how application of small fuzzification function models the relative importance of distances from host rocks. The application of small function results in a fuzzy evidence layer in which proximal of the rocks is more indicator than distal and so were assigned by higher weights to prospect orogenic gold deposits.

5.1.5 Metal deposition evidence map

Geochemical signatures have been used to prospect orogenic-gold deposits in regional-scale explorations (Nykänen et al., 2008b; Nykänen and Salmirinne 2007; Bierlein and McKnight 2005; Fu et al., 2012; Groves et al., 2000; Goldfarb et al., 2001). In the study area of this paper, based on available data, we used stream sediment uni-element concentration data of As, Au, and Bi reflecting sulfide sources and gold occurrences (cf. Goldfarb et al., 2001; Nykänen et al., 2008b) to generate a metal deposition evidence layer for MPM. These elements have been used to study orogenic gold deposits and are associated with this type of mineralization worldwide and in the study area (Groves et al., 2000; Goldfarb et al., 2001; Aliyari et al., 2007, 2009, 2012; Nykänen et al., 2008b; Almasi et al., 2015b). For modeling geochemical anomalies representing gold mineralization in the study area, concentration values of the selected elements were transformed into logistic space. Transformation of the values of stream sediment geochemical signatures into a logistic space, compared using original space (i.e., raw data), not only allows for better discrimination of geochemical anomalies but also improves the prediction-rate of mineral occurrences (Yousefi et al., 2014; Yousefi and Carranza, 2015a, b). For generating mono-element geochemical signature layers, we used logistically transformed-values of element concentrations (using Eq. [1]) instead of original raw data. Thus, geochemical anomalies of As, Au, and Bi elements lie on a common scale from 0 to 1 (Nykänen and Salmirinne (2007); Nykänen et al. (2008a); Yousefi and Carranza (2015b). From regional to district scale exploration program stream sediment data have been widely used to find mineralization signatures (e.g., Cheng, 2007; Cheng and Agterberg, 2009; Parsa et al., 2017a, b). After transformation of element concentrations, because each stream sediment sample is representative of its upstream composition (Bonham-Carter, 1994; Bonham-Carter and Goodfellow, 1984, 1986; Carranza and Hale, 1997; Moon, 1999; Spadoni et al., 2004; Spadoni, 2006; Carranza, 2008, 2010; Yousefi et al., 2013), a catchment basin modeling method was employed to portray geochemical anomalies (e.g. Bonham-Carter, 1994; Carranza, 2008). Based on Bonham-Carter and Goodfellow (1984, 1986) and Spadoni et al. (2004), the area of influence of each stream sediment sample is defined as the upstream areas. For this, we used drainage catchment basins (DCB) mapping technique (Yousefi et al., 2013) to modulate the negative effects of transported materials in delineation of

mineralization-related geochemical anomalies. We used concentration-area fractal model (Cheng et al., 1994) to define anomaly thresholds for leveling the data, and consequently, for ascertaining the relative importance of catchment basins. Then geochemical signature maps of As, Au, and Bi were combined by using Eq. [5] of Yousefi et al, 2012 to generate a geochemical mineralization prospectivity index, $GMPI_{Au\text{-}orogenic}$, as a stronger multi-element geochemical signature of orogenic gold deposition in the study area (Fig. 7a). In this paper, because the purpose is fuzzification of spatial relationship of indicator features and mineral deposits, the generated geochemical anomaly model has been presented as a fuzzy map rather than a classified model. Figure 7b shows that transformation of element concentrations using logistic function results in geochemical anomalies with more discrimination.

5.2. Integration of weighted evidence maps

After generation of weighted fuzzy evidence layers, they should be combined to generate target areas for further exploration of the mineral deposit-type sought (Bonham-Carter, 1994; Carranza, 2008). For this, regarding to the weighting methods, several mathematical functions can be used to combine evidence layers (Bonham-Carter, 1994; Carranza, 2008). In this paper, we used two combination functions, namely (i) fuzzy gamma operator (An et al., 1991; Bonham-Carter, 1994) and (ii) geometric average function (Yousefi and Carranza, 2015c). Either of these two functions can be used to combine fuzzified evidence maps regardless of how weights of evidence values were given. Figures 8a and 8b show the prospectivity models generated by fuzzy gamma and geometric average operators, respectively.

5.3. Evaluation of prospectivity models

Locations of known mineral deposits of the type sought in an area can be used as an empirical test to evaluate the results of prospectivity modeling in the area and to obtain measures of success (Agterberg and Bonham-Carter, 2005; Fabbri and Chung, 2008; Nykänen et al., 2015; Parsa et al., 2016a, b). We used the locations of seven known orogenic gold occurrences in the study area to evaluate the efficiency of the prospectivity models generated by using the two different methods, and consequently, the functions applied for weighting evidence values. For this, we used prediction-area (P-A) plot (Yousefi and Carranza, 2015b, 2016b) and success-rate curves (e.g., Agterberg and Bonham-Carter, 2005; Carranza and Laborte, 2015; Parsa et al., 2016a,b) (Fig. 9). The P-A plot has been drawn for each of the two above-mentioned prospectivity models. In a P-A plot, two curves namely prediction-rate curve of mineral deposits and occupied area curve are plotted in a scheme versus their corresponding prospectivity classes. Thus, the ability of the prospectivity model in terms of predicting larger number of mineral deposits in a smaller area is evaluated. The intersection point of the two curves that is a criterion to evaluate and compare the prospectivity models (Yousefi and Carranza, 2015b, 2016b) achieves this. Based on the intersection points in Fig. 9a, 86% of the known orogenic gold occurrences are predicted in 14% of the study area for the fuzzy prospectivity model

whereas 89% of the known orogenic gold occurrences are predicted in 11% of the study area (Fig. 9b) based on the geometric average prospectivity model. According to Yousefi and Carranza (2015b), the extracted parameters of the intersection point of the two curves (i.e., prediction-rate and occupied area) in the P-A plots can be used to calculate normalized density, N_d, and the efficiency (weight) of the prospectivity model, W_e. N_d is calculated as the prediction-rate of a prospectivity model divided by its corresponding occupied area extracted from the intersection point of the P-A plot, and W_e is calculated by taking the natural logarithm of N_d (Mihalasky and Bonham-Carter, 2001, Yousefi and Carranza, 2015b). The values of N_d and W_e for the geometric average prospectivity model are 8.09 and 2.09, respectively while for the fuzzy prospectivity model they are 6.14 and 1.81, respectively.

For further evaluation of the generated prospectivity models, we used a modified success-rate curve with a gauge line (N_d=1) proposed by Parsa et al. (2016a) as well. The success-rate curve (Chung and Fabbri, 2003; Agterberg and Bonham-Carter, 2005) is drawn by plotting the portion of mineral occurrences predicted correctly, P_o, in vertical axis versus the portion of the study area classified as prospective, P_a, in horizontal axis (e.g., Carranza and Laborte, 2015). In the modified success-rate curve the diagonal line, which represents N_d=1 and W_e=0, is a criterion for evaluation the relative importance of prospectivity models (Parsa et al., 2016a). A value of N_d close to 1 for a class of prospectivity indicates that the class consists of randomly selected pixels and hence is an unsupportive prediction class (Chung and Fabbri, 2003). Thus, the diagonal line on the plot of the success-rate curve is a gauge line for separating efficient and inefficient prospectivity models. In this regard, if the success-rate curve of a prospectivity model appears under the gauge line, it represents negative spatial association of the model with the mineralization and thus, the model is not a good-generated target area for prospecting the deposit-type sought. On the other hand, if the success-rate curve of a model appears above the gauge line, it represents positive spatial association of the model with the mineralization and thus, the model is an efficient model to prospect the deposit-type sought. This is because a value of $N_d > 1$ ($W_e > 0$) for a prospectivity model, indicates a positive association of the generated target areas with the mineralization of the type sought, while a value of $N_d < 1$ ($W_e < 0$) for a model of mineral prospectivity, indicates a negative association of the targets with the mineralization of the type sought (Mihalasky and Bonham-Carter, 2001, Yousefi and Carranza, 2015b). In addition, if the success-rate curve of a certain prospectivity model appears in higher above the gauge line in comparison with the success-rate curves of other prospectivity models, it represents that the generated target areas have better spatial association with the mineralization. The success-rate curve for both of the prospectivity models (Fig. 9c) appear above the gauge line. Thus, these two models are efficient to generate target areas of the deposit-type sought. However, success-rate curve of geometric average model appears in higher above the gauge line in comparison with the success-rate curves of fuzzy prospectivity model.

The above-mentioned comparisons illustrate that target areas with high prospectivity values based on the geometric average prospectivity model have priority for further exploration rather than those based on the fuzzy prospectivity model.

6. Discussion

The characteristics of a certain type of mineral deposit can be different in different areas. Such differences, which are a function of individual mineralization-related factors, are related to geological complexity associated with mineralization in the area. Therefore, understanding mineral system processes of the deposit-type sought in the area facilitates eliciting of exploration features to be used for MPM. In this regard, diversity of relationships between various mineral deposits and their corresponding spatial evidence values results in different conceptual models of mineral prospectivity. Thus, translation of the parameters of a conceptual model, which derived from understanding mineral system of the corresponding deposit-type sought, to weighted evidence layers is a critical undertaking (e.g., McCuaig et al., 2010; Joly et al., 2012). The weighted evidence layers would represent the diverse relationships between the mineral deposit-type sought and the evidence data. As demonstrated in this paper, the different relationships can be modeled by different logistic functions however, locations of known mineral occurrences are not used as training points and spatially continuous evidential values are not discretized using arbitrary intervals. Furthermore, by recognizing the mineralization-related factors elicited from understanding of mineral system processes of the deposit-type sough in the study area, we facilitated the decision-making for generation and prioritization of exploration targets.

Considering the proposed methods in this paper, when lower spatial evidence values, e.g., a depletion of a geochemical element and proximal to a certain geological feature, are indicators for prospecting mineral deposits, the small fuzzification function can be used efficiently to generate weighted evidence layer. On the other hand, when higher spatial evidence values, e.g., enrichment of a geochemical element, high values of geophysical magnetic intensity, and high fault density values, are indicators for prospecting mineral deposits, application of the large fuzzification function resulted in fuzzy scores, which lied in [0, 1] range. However higher values of spatial evidence given higher weights close to 1 and lower values of spatial evidence given lower weights close to 0. In the situations that intermediate values of spatial evidence are indicators, the near fuzzification function, as explained in the method section, can be applied.

There are various type of uncertainties that adversely affect prospectivity analysis of mineral deposits (e.g., McCuaig et al., 2010; Yousefi and Carranza, 2015a), of which the noteworthy are: (a) uncertainty due to missing evidence (Zuo et al., 2015); (b) uncertainty resulting from imprecise weighting to spatial evidence values (e.g., Nykänen et al. 2008a; Yousefi and Nykänen, 2016; Yousefi, 2017); (c) uncertainty in selection of subjectively-defined functions to be used for weighting spatial values (Luo, 1990; Luo and Dimitrakopoulos, 2003); (d) uncertainty due to complexity of geological setting (Van Loon, 2002) and anomaly patterns (Cheng, 2007; Yousefi et al., 2013); (e) uncertainty due to dissimilarities of geological settings (McCuaig et al., 2010; Lisitsin et al., 2013); (f) uncertainties due to incomplete knowledge in the understanding of mineral system processes (McCuaig et al., 2010); (f) uncertainty due to complex relationships between indicator features and mineral deposits (e.g., Yousefi et al., 2013), and (g) uncertainty due to inaccurately and imprecisely

presenting of geological features in exploration datasets (Lisitsin et al., 2013). Fuzziness, probability, similarity, vagueness, randomness, ambiguity, possibility, and imprecision are other types or sources of uncertainty as well (Celikyilmaz and Burhan Türksen, 2009; Yousefi and Carranza, 2015a). In this paper, we modulated the exploration bias resulting from improper selection of logistic function to be used for assigning evidential weights. However, further works are needed to overcome completely the other above-mentioned types of exploration bias and uncertainties to be used for prospectivity analysis.

Prospectivity analysis of orogenic gold deposits in Saqez-Sardasht goldfield demonstrated, however, that the SSZ has a NW–SE trend, considering the spatial distribution pattern of known gold deposits in the study area, a NE–SW trend can be recognized for the mineralization events (Fig. 8). Consequently, areas with high prospectivity values in Figure 8, which show the above-mentioned trend, have priority for further explorations.

7. Concluding remarks

- Considering the conceptual model of orogenic gold deposits and the various relationships between exploration features and system of mineralization, logistic-based fuzzification functions can be competently used to translate geological characteristics of the mineralization into exploration evidence layers.
- Various type of relationships between exploration features and a mineralization-type sought can be quantified using different fuzzification functions, i.e., small, large, and near functions. For a certain type of exploration data, a proper logistic function must be applied respecting the kind of relationship.
- Prospectivity modeling of orogenic gold mineralization in the study area shows that the E–W to ENE–WSW trending targets should be prioritized for further prospecting of the deposits.
- However, there are general indicator features that can be used to make a conceptual model for prospecting a certain deposit-type sough in a study area, understanding of mineral system processes of the deposit and translation of the processes into weighted evidence layers using proper mathematical functions are important keys to elicit mineralization-related exploration features for prospectivity analysis.

Acknowledgements

The authors express special thanks to Dr. Hasan Kheyrolahi and Dr. Alireza Jafarirad for some supports. The authors appreciate Dr. Hossein Tajeddin because field operations were carried out by him. We deeply appreciate the constructive comments of two anonymous reviewers, which helped us improve this paper.

References

Agterberg, F.P. and Bonham-Carter, G.F., 2005. Measuring the performance of mineral-potential maps. Natural Resources Research 14, 1-17.

Airo M. L. 2001. Aeromagnetic and aeroradiometric response to hydrothermal alteration. Surveys in Geophysics 23, 273-302.

Airo M. L. 2007. Application of aerogeophysical data for gold exploration: implications for the central lapland greenstone belt. Geological Survey of Finland, Special Paper 44, 187-208.

Akima, H., 1970: A new method of interpolation and smooth curve fitting based on local procedures. Journal of Association for Computing Machinery 17, 589-602.

Alavi, M., 1980, Tectonostratigraphic evolution of the Zagrosides of Iran: Geology 8, 144–149.

Alavi, M., 1994, Tectonics of the Zagros orogenic belt of Iran: new data and interpretations: Tectonophysics 229, 211–238.

Aliyari, F., 2006, Mineralogy, geochemistry and fabrics of gold mineralization in ductile to brittle shear zones of Qolqoleh deposit, southwest of Saqez, Iran: M.Sc. thesis, Tarbiat Modares University, Tehran, Iran.

Aliyari F., Rastad E., Arehart G. B. 2009. Geology and geochemistry of D-O-C isotope systematics of the Qolqoleh Gold Deposit, Northwestern Iran; implications for ore genesis. Ore Geology Reviews 36, 306-314.

Aliyari F., Rastad E., Mohajjel M. 2012. Gold Deposits in the Sanandaj-Sirjan Zone: Orogenic Gold Deposits or Intrusion-Related Gold systems? Resource Geology 62, 296-315.

Aliyari F., Rastad E., Zengqian H. 2007. Orogenic Gold Mineralization in the Qolqoleh Deposit, Northwestern Iran. Resource Geology 57, 269-282.

Almasi A., Jafarirad A., Kheyrollahi H., Rahimi M., Afzal P., 2014. Evaluation of structural and geological factors in orogenic gold type mineralization in the Kervian area, north-west Iran, using airborne geophysical data. Exploration Geophysics 45, 261-270.

Almasi, A., Jafarirad, A., Afzal, P., Rahimi, M., 2015a. Orogenic Gold Prospectivity Mapping Using Geospatial Data Integration, Region of Saqez, NW of Iran, Bulletin of the Mineral Research and Exploration 150, 65-76.

Almasi, A., Jafarirad, A., Afzal, P., Rahimi, M., 2015b. Prospecting of gold mineralization in Saqez area (NW Iran) using geochemical, geophysical and geological studies based on multifractal modelling and principal component analysis, Arabian Journal of Geosciences (8-8) 5935-5947.

Alpaydm, E., 2004. Introduction to Machine Learning. The MIT Press, Cambridge, Massachusetts.

An, P., Moon, W.M., Rencz, A., 1991, Application of fuzzy set theory for integration of geological, geophysical and remote sensing data. Canadian Journal of Exploration Geophysics 27, 1–11.

Archibald, N., Gow, P., and Boschetti, F., 1999. Multiscale edge analysis of potential field data. Exploration Geophysics 30, 38-44.

Asadi, H.H., Porwal, A., Fatehi, M., Kianpouryan, S., Lu, Y.J., 2015. Exploration feature selection applied to hybrid data integration modeling: Targeting copper-gold potential in central Iran. Ore Geology Reviews, 71, 819–838.

Asadi, H.H., Sansoleimani, A., Fatehi, M., Carranza, E.J.M., 2016. An AHP–TOPSIS predictive model for district-scale mapping of porphyry Cu–Au potential: a case study from Salafchegan Area (Central Iran). Natural Resources Research 25, 417-429.

Austin, J. R., Blenkinsop, T. G., 2008. The Cloncurry Lineament: geophysical and geological evidence for a deep crustal structure in the Eastern Succession of the Mount Isa Inlier: Precambrian Research 163, 50-68.

Austin, J. R., Blenkinsop, T. G., 2009. Local to regional scale structural controls on mineralisation and the importance of a major lineament in the eastern Mount Isa Inlier, Australia: review and analysis with autocorrelation and weights of evidence: Ore Geology Reviews 35, 298-316.

Babakhani A. R., Hariri A., Farjandi F. 2003. Geological map of Saqez (1:100000 scale). Geological Survey of Iran (GSI).

Baranov, V., 1957. A new method for interpretation of aeromagnetic maps: pseudo-gravimetric anomalies: Geophysics 22, 359-382.

Bark, G., Weihed, P., 2012. Geodynamic settings for Paleoproterozoic gold mineralization in the Svecofennian domain: A tectonic model for the Fäboliden orogenic gold deposit, northern Sweden. Ore Geology Reviews 48, 403-412.

Beaudoin, G., Therrien, R., Savard, C., 2006. 3D numerical modelling of fluid flow in the Val-d'Or orogenic gold district: major crustal shear zones drain fluids from overpressured vein fields. Mineralium Deposita, 41:82.

Berberian, M., King, G.C.P., 1981. Towards a paleogeography and tectonic evolution of Iran. Canadian Journal of Earth Sciences 18, 210-265.

Berthold, M., Hand, D.J. 2002. Intelligent Data Analysis. 2nd Ed., Springer- Verlag, Berlin Heidelberg.

Betts, P. G., Lister, G. S., 2002. Geodynamically indicated targeting strategy for shale-hosted massive sulfide Pb–Zn–Ag mineralisation in the Western Fold Belt, Mt. Isa terrane: Australian Journal of Earth Sciences 49, 985-1010.

Bierlein F. P., Murphy F. C., Weinberg R. F. & Lees T. 2006a. Distribution of orogenic gold deposits in relation to fault zones and gravity gradients: targeting tools applied to the Eastern Goldfields, Yilgarn Craton, Western Australia. Mineralium Deposita 41, 107-126.

Bierlein F. P., Groves, D.I., Goldfarb. R.J., Dubé, B., 2006b. Lithospheric controls on the formation of provinces hosting giant orogenic gold deposits. Mineralium Deposita, 40:874.

Bierlein, F.P., McKnight, S., 2005. Possible intrusion-related gold systems in the western Lachlan Orogen, southeast Australia. Economic Geology 100, 385-398.

Bishop, C.M. 2006. Pattern Recognition and Machine Learning. Springer Science+Business Media. LLC, 233 Spring Street, New York, NY 10013, USA.

Bonham-Carter, G.F. 1994. Geographic Information Systems for Geoscientists: Modelling with GIS. Pergamon, Oxford.

Bonham-Carter, G.F., Goodfellow, W.D., 1984. Autocorrelation structure of stream-sediment geochemical data: interpretation of Zn and Pb anomalies, Nahanni River area, Yukon-Northwest Territories, Canada. Geostatistics for natural resources characterization, pt, 2, pp.817-829.

Bonham-Carter, G.F., Goodfellow, W.D., 1986. Background corrections to stream geochemical data using digitized drainage and geological maps: application to Selwyn Basin, Yukon and Northwest Territories. Journal of Geochemical Exploration 25, 139-155.

Burrough, P.A., McDonnell, R.A., 1998. Principles of geographical information systems: New York, Oxford University Press, 333 p.

Carranza, E.J.M., 2008. Geochemical Anomaly and Mineral Prospectivity Mapping in GIS. Handbook of Exploration and Environmental Geochemistry, Vol. 11. Elsevier, Amsterdam.

Carranza, E.J.M., 2009. Objective selection of suitable unit cell size in data-driven modeling of mineral prospectivity. Computers & Geosciences 35, 2032-2046.

Carranza, E.J.M., 2010. Mapping of anomalies in continuous and discrete fields of stream sediment geochemical landscapes. Geochemistry: Exploration, Environment, Analysis 10, 171-187.

Carranza, E.J.M., 2014. Data-driven evidential belief modeling of mineral potential using few prospects and evidence with missing values. Natural Resources Research 24, 291-304.

Carranza, E.J.M., 2017. Natural Resources Research publications on geochemical anomaly and mineral potential mapping, and introduction to the special issue of papers in these fields. Natural Resources Research 26, 379-410.

Carranza, E.J.M., Hale, M., 2001. Geologically-constrained fuzzy mapping of gold mineralization potential, Baguio district, Philippines. Natural Resources Research 10, 125–136.

Carranza, E.J.M., Hale, M., 2002. Where are porphyry copper deposits spatially localized? A case study in Benguet province, Philippines. Natural Resources Research 11, 45-59.

Carranza, E.J.M., Laborte, A.G., 2016. Data-driven predictive modeling of mineral prospectivity using Random Forests: a case study in Catanduanes Island (Philippines). Natural Resources Research 25, 35-50.

Carranza, E.J.M., Sadeghi, M., Billay, A., 2015. Predictive mapping of prospectivity for orogenic gold, Giyani greenstone belt (South Africa). Ore Geology Reviews 71, 703-718.

Carranza, E.J.M., Woldai, T., Chikambwe, E. M., 2005. Application of Data-Driven Evidential Belief Functions to Prospectivity Mapping for Aquamarine-Bearing Pegmatites, Lundazi District, Zambia. Natural Resources Research 14, 47-63.

Carranza, E.J.M., Laborte, A.G., 2015. Random forest predictive modeling of mineral prospectivity with small number of prospects and data with missing values in Abra (Philippines). Computers & Geosciences, 74, pp.60-70.

Carranza, E.J.M., Hale, M., 1997. A catchment basin approach to the analysis of reconnaissance geochemical-geological data from Albay Province, Philippines. Journal of Geochemical Exploration 60, 157-171.

Celikyilmaz , A., Burhan Türksen, I., 2009. Modeling uncertainty with fuzzy logic, Springer-Verlag Berlin Heidelberg.

Cheng, Q., 2007. Mapping singularities with stream sediment geochemical data for prediction of undiscovered mineral deposits in Gejiu, Yunnan Province, China. Ore Geology Reviews 32, 314-324.

Cheng, Q., Agterberg, F.P., 1999, Fuzzy weights of evidence method and its application in mineral potential mapping. Natural Resources Research 8, 27-35.

Cheng, Q., Agterberg, F.P., 2009. Singularity analysis of ore-mineral and toxic trace elements in stream sediments. Computers and Geosciences 35, 34–244.

Cheng, Q., Agterberg, F.P., Ballantyne, S.B., 1994. The separation of geochemical anomalies from background by fractal methods. Journal of Geochemical Exploration 51, 109–130.

Chung, C.J.F. and Fabbri, A.G., 2003. Validation of spatial prediction models for landslide hazard mapping. Natural Hazards 30, 451-472.

Coolbaugh, M. F., Raines, G. L., Zehner, R. E., 2007. Assessment of Exploration Bias in Data-Driven Predictive Models and the Estimation of Undiscovered Resources. Natural Resources Research 16, 199-207.

Craw, D., Begbie, M., MacKenzie, D., 2006. Structural controls on Tertiary orogenic gold mineralization during initiation of a mountain belt, New Zealand. Mineralium Deposita, 41(7), 645-659.

Cross, A.J., Fletcher, I.R., Crispe, A.J., Huston, D.L., Williams, N., 2005. New constraints on the timing of deposition and mineralisation in the Tanami Group (abstract). Northern Territory Geological Survey record 2005–001.

De Quadros, T.F.P., Koppe, J.C., Strieder, A. J., Costa, J. F. C. L., 2003. Gamma-Ray Data Processing and Integration for Lode-Au Deposits Exploration. Natural Resources Research 12, 57-65.

De Souza Filho, C.R., Nunes, A.R., Leite, E.P., Monteiro, L.V.S., Xavier, R.B., 2007. Spatial analysis of airborne geophysical data applied to geological mapping and mineral prospecting in the Serra Leste region, Caraja´s Mineral Province, Brazil. Surveys in Geophysics 28, 377-405.

Duarte Campos, L., Machado de Souza, S., Alves de Sordi, D., Mattos Tavares, F., Klein, E.L., dos Santos Lopes, E.C., 2017. Predictive mapping of prospectivity in the Gurupi Orogenic Gold Belt, North–Northeast Brazil: an example of district-scale mineral system approach to exploration targeting. Natural Resources Research, DOI:10.1007/s11053-016-9320-5.

Eftekharnejad, J., 1981. Tectonic division of Iran with respect to sedimentary basins. Journal of Iranian Petroleum Society, 82, 19-28 (in Persian).

Ferreira F., de Castro L., Bongiolo A., de Souza J. & Romeiro M. 2011. Enhancement of the total horizontal gradient of magnetic anomalies using tilt derivatives: Part II — Application to real data. SEG Technical Program Expanded Abstracts 2011, 887-891.

Fink, G.A. 2007. Markov Models for Pattern Recognition. Springer-Verlag, Berlin Heidelberg.

Ford, A., Miller, J.M., Mol, A.G., 2016. A Comparative Analysis of Weights of Evidence, Evidential Belief Functions, and Fuzzy Logic for Mineral Potential Mapping Using Incomplete Data at the Scale of Investigation. Natural Resources Research 25, 19-33.

Fraser, G., 2002. Geochronology of Tanami ores and host rocks. Northern Territory Geological Survey Record 2002/0003.

Fu, B., Kendrick, M.A., Fairmaid, A.M., Phillips, D., Wilson, C.J.L., Mernagh, T.P., 2012. New constraints on fluid sources in orogenic gold deposits, Victoria, Australia. Contributions to Mineralogy and Petrology 163, 427-447.

Ghasemi, A., Talbot, C. J., 2006, A new tectonic scenario for the Sanandaj–Sirjan Zone (Iran): Journal of Asian Earth Sciences 26, 683–693.

Goldfarb, R.J., Groves, D.I., 2015. Orogenic gold: Common or evolving fluid and metal sources through time. Lithos 233, 2-26.

Goldfarb, R.J., Groves, D.I., Gardoll, S., 2001. Orogenic gold and geologic time: a global synthesis. Ore Geology Reviews 18, 1-75.

Grauch, V.J.S., Rodriguez, B.D., Wooden, J.L., 2003. Geophysical and Isotopic Constraints on Crustal Structure Related to Mineral Trends in North-Central Nevada and Implications for Tectonic History. Economic Geology 98, 269-286.

Groves, D.I., 1993. The crustal continuum model for Late-Archaean lode-gold deposits of the Yilgarn Block, Western Australia. Mineralium Deposita 28, 366-374.

Groves, D.I., Goldfarb, R.J., Gebre-Mariama, M., Hagemann, S.G., Robert, F., 1998. Orogenic gold deposits: A proposed classification in the context of their crustal distribution and relationship to other gold deposit types. Ore Geology Reviews 13, 7-27.

Groves, D.I., Goldfarb, R.J., Knox-Robinson, C.M., Ojala, J., Gardoll, S., Yun, G.Y., Holyland, P., 2000. Late-kinematic timing of orogenic gold deposits and significance for computer-based exploration techniques with emphasis on the Yilgarn Block, Western Australia. Ore Geology Reviews 17, 1-38.

Haynes D.W., 2000. Iron oxide copper (-gold) deposits: their position in the ore deposit spectrum and modes of origin. In: Porter TM (ed) Hydrothermal iron oxide copper-gold and related deposits: A global perspective. Australian Mineral Foundation, Adelaide, 71-90.

Heidari S. M., Rastad E., Mohajjel M. Shamsa M. J. 2006. Gold mineralization in ductile shear zone of Kervian (southwest of Saqez-Kordestan province). Geosciences 58, 18-37.

Heidari S. M. 2004. Mineralogy, geochemistry and fabrics of gold mineralization in the Kervian ductile shear zone (southwest of Saqez, Kordestan province). University of Tarbiat Modares, Tehran, Iran, M.Sc. thesis, 245 pp (in Persian).

Hengl, T., 2006. Finding the right pixel size. Computers & Geosciences 32, 1283–1298.

Henson, P. A., Blewett, R. S., Roy, I. G., Miller, J. McL., Czarnota, K., 2010. 4D architecture and tectonic evolution of the Laverton region, eastern Yilgarn Craton, Western Australia: Precambrian Research 183, 338-355.

Herbert, S., Woldai, T., Carranza, E.C.M., van Ruitenbeek, F.J.A., 2014. Predictive mapping of prospectivity for orogenic gold in Uganda. Journal of African Earth Sciences 99, 666-693.

Holden, D., Archibald, N. J., Boschetti, F., and Jessell, M. W., 2000. Inferring geological structures using wavelet-based multiscale edge analysis and forward models: Exploration Geophysics 31, 617-621.

Joly, A., Porwal, A., McCuiag, T.C., 2012. Exploration targeting for orogenic gold deposits in the Granites-Tanami Orogen: Mineral system analysis, targeting model and prospectivity analysis. Ore Geology Reviews 48, 349-383.

Kemp, L., Bonham-Carter, G.F., Raines, G.L., and Looney, C.G., 2001, ArcSDM and DataXplore – spatial data modeler for Arcview and Spatial Analyst http://ntserv.gis.nrcan.gc.ca/sdm/.

Knox-Robinson, C.M., 2000. Vectorial fuzzy logic: a novel technique for enhanced mineral prospectivity mapping, with reference to the orogenic gold mineralisation potential of the Kalgoorlie Terrane, Western Australia. Australian Journal of Earth Sciences 47, 929-941.

Li, L., 2013. Improved edge detection tools in the interpretation of potential field data: Exploration Geophysics 44, 128-132.

Lisitsin, V.A., González-Álvarez, I., Porwal, A., 2013. Regional prospectivity analysis for hydrothermal-remobilised nickel mineral systems in western Victoria, Australia. Ore Geology Reviews 52, 100-112.

Lisitsin, V.A., Moore, D.H., Olshina, A., Willman, C.E., 2010. Undiscovered orogenic gold endowment in Northern Victoria, Australia. Ore Geology Reviews 38, 251–269.

Luo, J., 1990. Statistical mineral prediction without defining a training area. Mathematical Geology 22, 253-260.

Luo, X., Dimitrakopoulos, R., 2003. Data-driven fuzzy analysis in quantitative mineral resource assessment. Computers & Geosciences 29, 3–13.

Lusty, P.A.J., Scheib, C., Gunn, A.G., Walker, A.S.D., 2012. Reconnaissance-Scale Prospectivity Analysis for Gold Mineralisation in the Southern Uplands-Down-Longford Terrane, Northern Ireland. Natural Resources Research 21, 359-382.

Ma, G., and Li, L., 2012. Edge detection in potential fields with the normalized total horizontal derivative: Computers & Geosciences 41, 83-87.

Magalhães, L.A., Souza Filho, C.R., 2012. Targeting of Gold Deposits in Amazonian Exploration Frontiers using Knowledge- and Data-Driven Spatial Modeling of Geophysical, Geochemical, and Geological Data. Survey in Geophysics 33, 211-241.

Masters, T., 1993, Practical neural network recipes in C++: New York, Academic Press, p. 285.

McCuaig, T.C., Beresford, S., Hronsky, J., 2010. Translating the mineral systems approach into an effective targeting system. Ore Geol. Rev. 38, 128–138.

McKay, G., Harris, J.R., 2016. Comparison of the data-driven Random Forests model and a knowledge-driven method for mineral prospectivity mapping: a case study for gold deposits around the Huritz Group and Nueltin Suite, Nunavut, Canada. Natural Resources Research 25, 125-143.

Mejía-Herrera, P., Royer, J.J., Caumon, G., Cheilletz, A., 2014. Curvature attribute from surface-restoration as predictor variable in Kupferschiefer copper potentials. An example from the Fore-Sudetic Region. Natural Resources Research 24, 275-290.

Micheli-Tzanakou, E. 1999. Supervised and unsupervised Pattern Recognition. CRC Press LLC. Corporate Blvd., N.W., Boca Raton, Florida.

Mihalasky, M.J., Bonham-Carter, G.F., 2001, Lithodiversity and its spatial association with metallic mineral sites, Great Basin of Nevada. Natural Resources Research 10, 209-226.

Miller, H. G., Singh, V., 1994. Potential field tilt - a new concept for location of potential field sources: Journal of Applied Geophysics 32, 213-217.

Mohajjel, M., Fergusson, C.L., Sahandi, C.R., 2003. Cretaceous–Tertiary convergence and continental collision, Sanandaj–Sirjan Zone, western Iran. Journal of Asian Earth Sciences 21, 397-412.

Moon, C.J., 1999. Towards a quantitative model of downstream dilution of point source geochemical anomalies. Journal of Geochemical Exploration 65,111-132.

Murphy, J.B., Nance, R.D., 1992. Mountain belts and the supercontinent cycle. Scientific American 266, 84-91.

Mutele, L., Billay, A., Hunt, J.P., 2017. Knowledge-driven prospectivity mapping for granite-related polymetallic Sn–F–(REE) mineralization, Bushveld Igneous Complex, South Africa. DOI: 10.1007/s11053-017-9325-8.

Nykänen, V., 2008. Radial basis functional link nets used as a prospectivity mapping tool for orogenic gold deposits within the Central Lapland Greenstone Belt, Northern Fennoscandian Shield. Natural Resources Research 17, 29–48.

Nykänen, V., Niiranen, T., Molnár, F., Lahti, I., Korhonen, K., Cook, N., Skyttä, P., 2017. Optimizing a knowledge-driven prospectivity model for gold deposits within Peräpohja Belt, Northern Finland. Natural Resources Research, DOI:10.1007/s11053-016-9321-4.

Nykänen, V., Salmirinne, H., 2007. Prospectivity analysis of gold using regional geophysical and geochemical data from the Central Lapland Greenstone Belt, Finland. Geological Survey of Finland, Special Paper, 44, 251-269.

Nykänen, V., Groves, D.I., Ojala, V.J., Eilu, P., Gardoll, S.J., 2008a. Reconnaissance-scale conceptual fuzzy-logic prospectivity modelling for iron oxide copper–gold deposits in the Northern Fennoscandian Shield, Finland. Australian Journal of Earth Sciences 55, 25–38.

Nykänen, V., Groves, D.I., Ojala, V.J., Gardoll, S.J., 2008b. Combined conceptual/empirical prospectivity mapping for orogenic gold in the Northern Fennoscandian Shield, Finland. Australian Journal of Earth Sciences 55, 39–59.

Nykänen, V., Lahti, I., Niiranen, T., Korhonen, K., 2015. Receiver operating characteristics (ROC) as validation tool for prospectivity models—A magmatic Ni–Cu case study from the Central Lapland Greenstone Belt, Northern Finland. Ore Geology Reviews, 71, 853-860.

Parsa, M., Maghsoudi, A., Yousefi, M., Sadeghi, M., 2016a. Prospectivity modeling of Porphyry-Cu deposits by identification and integration of efficient mono-elemental geochemical signatures. Journal of African Earth Sciences 114, 228-241.

Parsa, M., Maghsoudi, A., Yousefi, M. and Sadeghi, M., 2016b. Recognition of significant multi-element geochemical signatures of porphyry Cu deposits in Noghdouz area, NW Iran. Journal of Geochemical Exploration 165, 111-124.

Parsa, M., Maghsoudi, A., Yousefi, M., Carranza, E.J.M., 2017a. Multifractal interpolation and spectrum–area fractal modeling of stream sediment geochemical data: Implications for mapping exploration targets. Journal of African Earth Sciences 128, 5-15.

Parsa, M., Maghsoudi, A., Yousefi, M., Sadeghi, M., 2017b. Multifractal analysis of stream sediment geochemical data: Implications for hydrothermal nickel prospection in an arid terrain, eastern Iran. Journal of Geochemical Exploration DOI: 10.1016/j.gexplo.2016.11.013.

Porwal, A, Carranza, E.J.M., Hale, M., 2004. A hybrid neuro-fuzzy model for mineral potential mapping. Mathematical Geology 36, 803-826.

Porwal, A., Carranza, E.J.M., Hale, M., 2003a. Extended weights-of-evidence modelling for predictive mapping of base metal deposit potential in Aravalli province, western India. Exploration and Mining Geology 10, 155-163.

Porwal, A., Carranza, E.J.M., Hale, M., 2003b. Artificial neural networks for mineral potential mapping: A Case Study from Aravalli Province, Western India. Natural Resources Research 12, 155-171.

Porwal, A., Carranza, E.J.M., Hale, M., 2003c. Knowledge-driven and data-driven fuzzy models for predictive mineral potential mapping. Natural Resources Research 12, 1-25.

Porwal, A., Carranza, E.J.M., Hale, M., 2006. A hybrid fuzzy weights-of-evidence model for mineral potential mapping. Natural Resources Research 15, 1-14.

Porwal, A., Kreuzer, O.P., 2010. Introduction to the Special Issue: Mineral prospectivity analysis and quantitative resource estimation, Ore Geology Reviews 38, 121-127.

Salem, A., Williams, S., Fairhead, J.D., Ravat, D., Smith, R., 2007. Tiltdepth method: a simple depth estimation method using first-order magnetic derivatives: The Leading Edge 26, 1502-1505.

Sillitoe, R.H., 2000. Gold-rich porphyry deposits: descriptive and genetic models and their role in exploration and discovery. Reviews in Economic Geology 13, 315-345.

Silva, A.M., Pires, A.C.B., Mccafferty, A., Moraes, R.A.V., Xia, H., 2003. Application of airborne geophysical data to mineral exploration in the uneven exposed terrains of the Rio das Velhas greenstone belt. Revista Brasileira de Geociências, 33, 17-28.

Smith, W.H.F., Wessel, P., 1990. Gridding with continuous curvature splines in Tension., Geophysics 55, 293-305.

Spadoni, M., 2006. Geochemical mapping using a geomorphologic approach based on catchments. Journal of Geochemical Exploration 90, 183-196.

Spadoni, M., Cavarretta, G., Patera, A., 2004. Cartographic techniques for mapping the geochemical data of stream sediments: the “sample catchment basin” approach. Environmental Geology 45, 593-599.

Stocklin, J., 1968. Structural History and Tectonics of Iran: A Review. AAPG (American Association of Petroleum Geologists) Bulletin, 52, 1229-1258.

Tajeddin, H., 2011. Gold ore controlling factors in metamorphic rocks of Saqez-Sardasht, NW of Sananda-Sirjan metamorphic zone. Tarbiat Modarres University, Tehran, Iran, PhD dissertation, 436 pp (in Persian).

Takin, M., 1972. Iranian Geology and Continental Drift in the Middle East. Nature, 235, 147-150.

Theodoridis, S., Koutroumbas, K., 2006. Clustering: basic concepts. Pattern Recognition, 483-516.

Thompson, M., Howarth, R.J., 1976. Duplicate analysis in geochemical practice. Part 1: theoretical approach and estimation of analytical reproducibility. Analyst 101, 690–698.

Tsoukalas, L.H., Uhrig, R.E., 1997. Fuzzy and Neural Approaches in Engineering, John Wiley & Sons, New York, NY, 606 p.

Van Loon, A.J., 2002. The complexity of simple geology. Earth-Science Reviews 59, 287–295.

Verduzco, B., Fairhead, J. D., Green, C. M., MacKenzie, C., 2004. New insights into magnetic derivatives for structural mapping: The Leading Edge, 23, 116-119.

Yousefi, M., 2017. Recognition of an enhanced multi-element geochemical signature of porphyry copper deposits for vectoring into mineralized zones and delimiting exploration targets in Jiroft area, SE Iran. Ore Geology Reviews 83, 200-214.

Yousefi, M., Carranza, E.J.M., 2015a. Fuzzification of continuous-value spatial evidence for mineral prospectivity mapping. Computers & Geosciences 74, 97-109.

Yousefi, M., Carranza, E. J. M., 2015b. Prediction-area (P-A) plot and C-A fractal analysis to classify and evaluate evidential maps for mineral prospectivity modeling. Computers & Geosciences 79, 69-81.

Yousefi, M., Carranza, E.J.M., 2015c. Geometric average of spatial evidence data layers: A GIS-based multi-criteria decision-making approach to mineral prospectivity mapping. Computers & Geosciences 83, 72–79.

Yousefi, M., Carranza, E. J. M., 2016a. Data-driven index overlay and Boolean logic mineral prospectivity modeling in greenfields exploration. Natural Resources Research 25, 3-18.

Yousefi, M., Carranza., E.J.M., 2016b. Union score and fuzzy logic mineral prospectivity mapping using discretized and continuous spatial evidence values. Journal of African Earth Sciences DOI: 10.1016/j.jafrearsci.2016.04.019.

Yousefi, M., Kamkar-Rouhani, A., Carranza, E.J.M. 2012. Geochemical mineralization probability index (GMPI): a new approach to generate enhanced stream sediment geochemical evidential map for increasing probability of success in mineral potential mapping. Journal of Geochemical Exploration 115, 24-35.

Yousefi, M., Carranza, E.J.M., and Kamkar-Rouhani, 2013. Weighted drainage catchment basin mapping of stream sediment geochemical anomalies for mineral potential mapping. Journal of Geochemical Exploration 128, 88-96.

Yousefi, M., Kamkar-Rouhani, A. and Carranza, E.J.M. 2014. Application of staged factor analysis and logistic function to create a fuzzy stream sediment geochemical evidence layer for mineral prospectivity mapping. Geochemistry: Exploration, Environmental, Analysis 14, 45-58.

Yousefi, M., Nykänen, V, 2016. Data-driven logistic-based weighting of geochemical and geological evidence layers in mineral prospectivity mapping. Journal of Geochemical Exploration 164, 94-106.

Zadeh, L.A., 1993. Fuzzy logic, neural networks and soft computing. In Safety Evaluation Based on Identification Approaches Related to Time-Variant and Nonlinear Structures (pp. 320-321). Vieweg+ Teubner Verlag.

Zuo, R., 2012. Exploring the effects of cell size in geochemical mapping. Journal of Geochemical Exploration 112, 357–367.

Zuo, R., Zhang, Z., Zhang, D., Carranza, E.J.M. and Wang, H., 2015. Evaluation of uncertainty in mineral prospectivity mapping due to missing evidence: a case study with skarn-type Fe deposits in Southwestern Fujian Province, China. Ore Geology Reviews, 71, 502-515.

Figure captions:

Fig. 1. Main tectonic units of Iran and the location of the study area in Sanandaj–Sirjan Zone (a), Saqez-Sardasht goldfield and broad distribution of the major gold deposit/prospects in the northern Sanandaj–Sirjan Zone (b) (after Alavi, 1994; Ghasemi and Talbot, 2006), and Saqez 1:100000 scale geological map (c) (after Babakhani et al., 2003).

Fig. 2. a) Au-bearing chlorite-schists (Qareh-Char), b) chlorite-schists of Qareh-char, c) sulfide Au-bearing ore, yellow bands are mostly rock-forming minerals such as quartz and feldspar, darker parts are sulfide-bearing products of quartz + carbonate + biotite alteration (Qabaghloujeh), d) outcrop of Au-bearing silicic veins, e) Au particles in quartz + carbonate + biotite gangue (Qabaghloujeh), f) sulfide Au-bearing ore (Qabaghloujeh) black matters are biotite, g) Au particles in a quartz background (Hamzeh-Qarnein), h) Au-bearing mylonitic-granite with a 2 mm wide Au particle, yellow banded (Qolqoleh) (Tajeddin, 2011).

Fig. 3. Fuzzified evidence layer of heat source (a) and variation of weights, assigned by small fuzzification function, versus corresponding original evidence values (b).

Fig. 4. Fuzzy evidence layer of pathways (a) and variation of weights, assigned by large fuzzification function, versus corresponding original evidence values (b).

Fig. 5. Fuzzy evidence layer of hydrothermal activities (a) and variation of weights, assigned by large fuzzification function, versus corresponding original evidence values (b).

Fig. 6. Fuzzy evidence layer of ore raps (a) and variation of weights, assigned by small fuzzification function, versus corresponding original evidence values (b).

Fig. 7. Multi-element geochemical signature of orogenic gold deposition in the study area represented as geochemical mineralization prospectivity index, $GMPI_{Au\text{-}orogenic}$, fuzzified geochemical evidence layer (a) and histogram of the final GMPI values of orogenic gold deposits. The histogram of the final GMPI values shows two major populations meaning as Yousefi et al., (2012, 2014) demonstrated transformation of evidential values using logistic function facilitate recognition of geochemical patterns, anomalies, or populations.

Fig. 8. Prospectivity model generated by fuzzy gamma (a) and geometric average (b) operators.

Fig. 9. Prediction-area plot of fuzzy (a) and geometric average (b) prospectivity models and success-rate curves of the two prospectivity models (c).

Table captions:

Table 1. Mineral system parameters (in general) of orogenic gold deposits

Table 2. Characteristics of gold deposits/occurrences in the study area

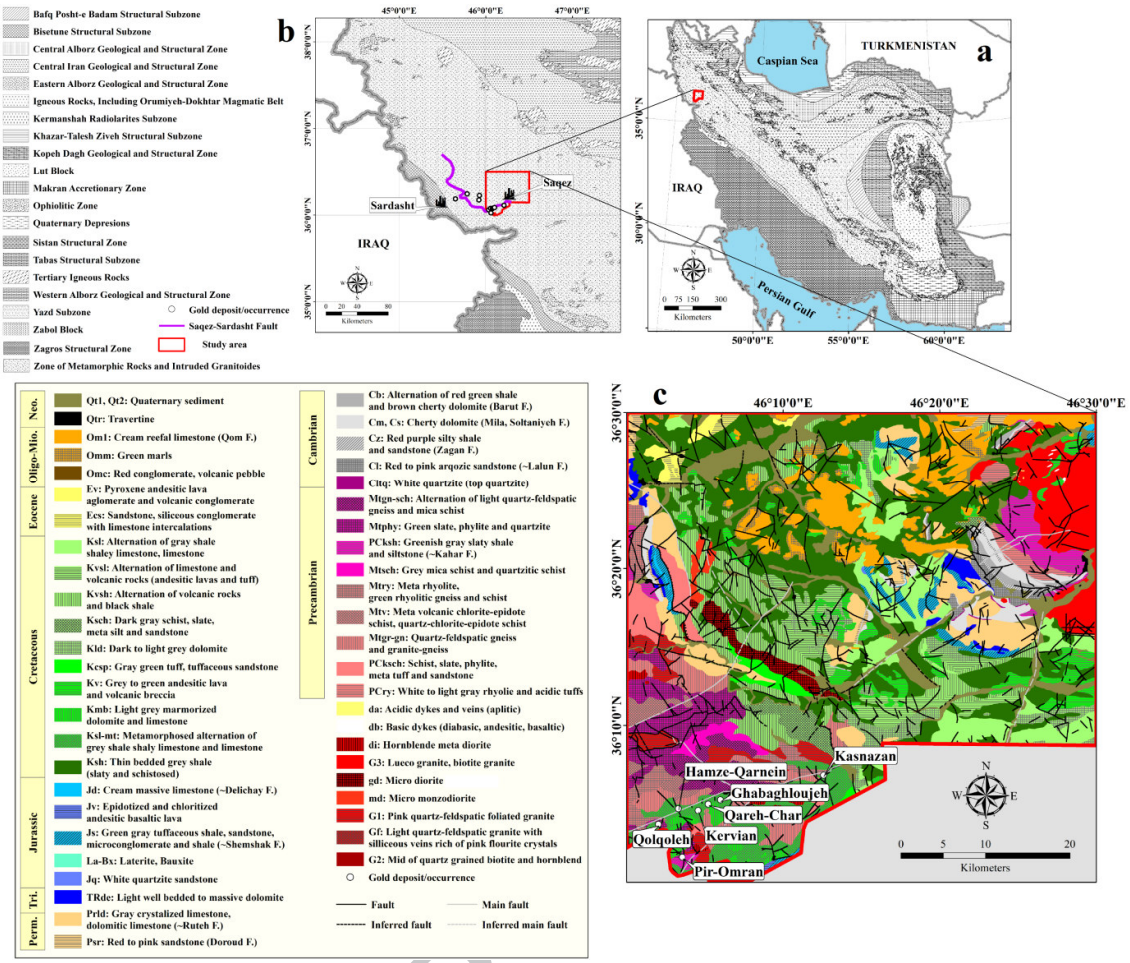

Fig. 1. Main tectonic units of Iran and the location of the study area in Sanandaj–Sirjan Zone (a), Saqez-Sardasht goldfield and broad distribution of the major gold deposit/prospects in the northern Sanandaj–Sirjan Zone (b) (after Alavi, 1994; Ghasemi and Talbot, 2006), and Saqez 1:100000 scale geological map (c) (after Babakhani et al., 2003).

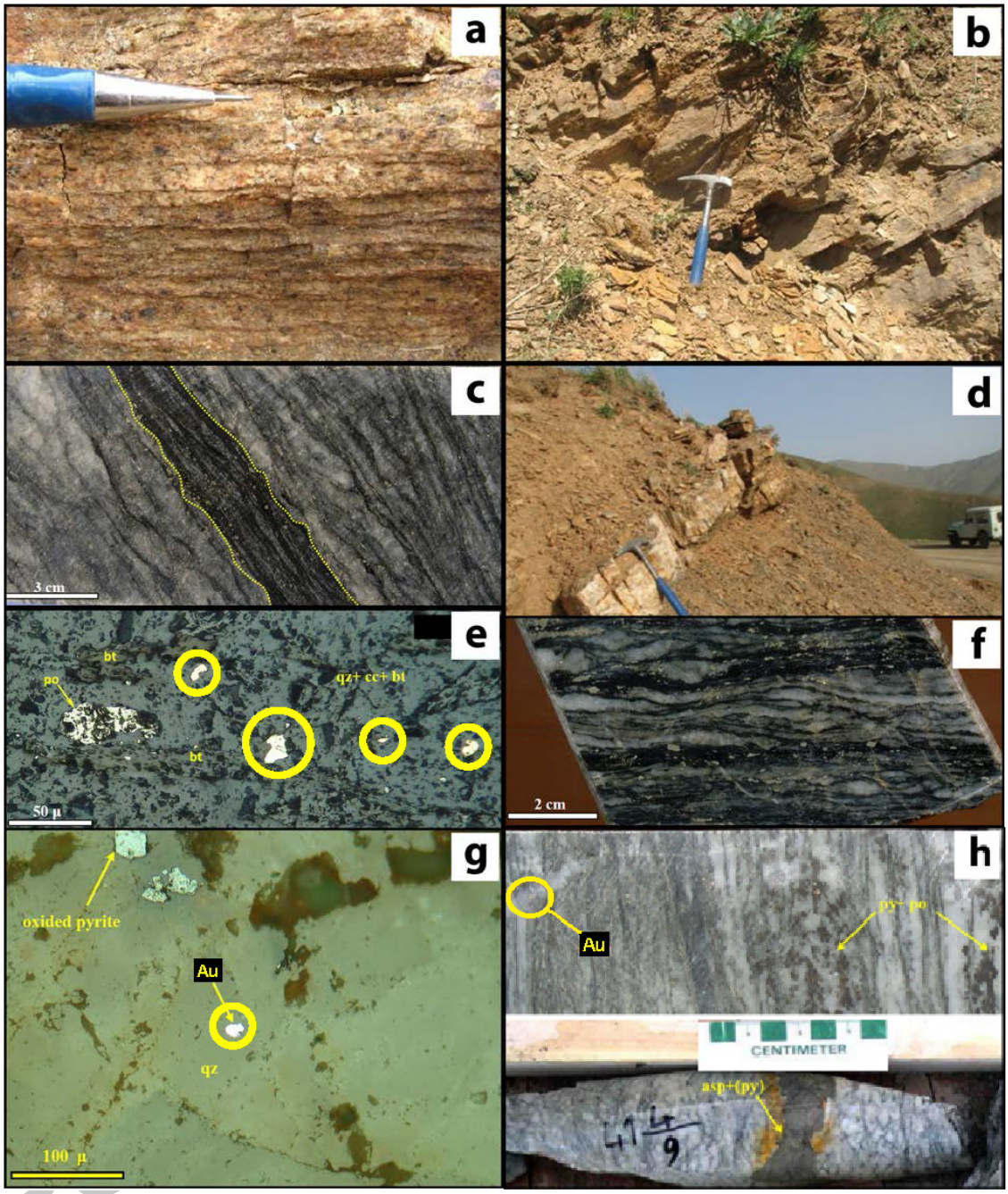

Fig. 2. a) Au-bearing chlorite-schists (Qareh-Char), b) chlorite-schists of Qareh-char, c) sulfide Au-bearing ore, yellow bands are mostly rock-forming minerals such as quartz and feldspar, darker parts are sulfide-bearing products of quartz + carbonate + biotite alteration (Qabaghloujeh), d) outcrop of Au-bearing silicic veins, e) Au particles in quartz + carbonate + biotite gangue (Qabaghloujeh), f) sulfide Au-bearing ore (Qabaghloujeh) black matters are biotite, g) Au particles in a quartz background (Hamzeh-Qarnein), h) Au-bearing mylonitic-granite with a 2 mm wide Au particle, yellow banded (Qolqoleh) (Tajeddin, 2011).

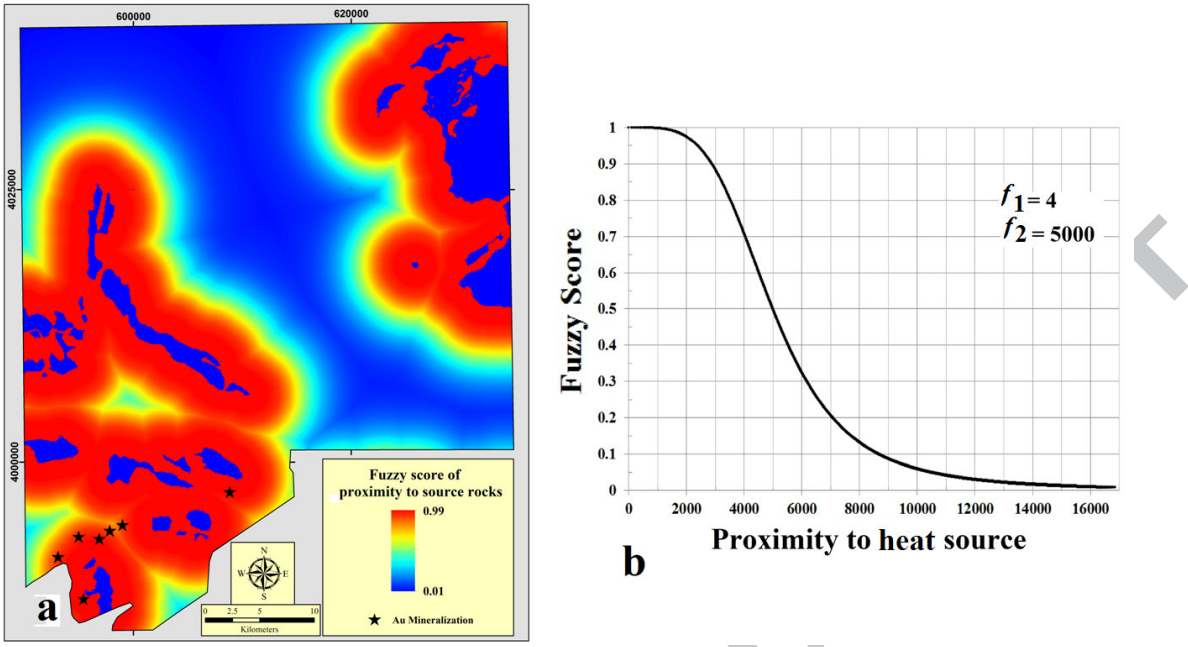

Fig. 3. Fuzzified evidence layer of heat source (a) and variation of weights, assigned by small fuzzification function, versus corresponding original evidence values (b).

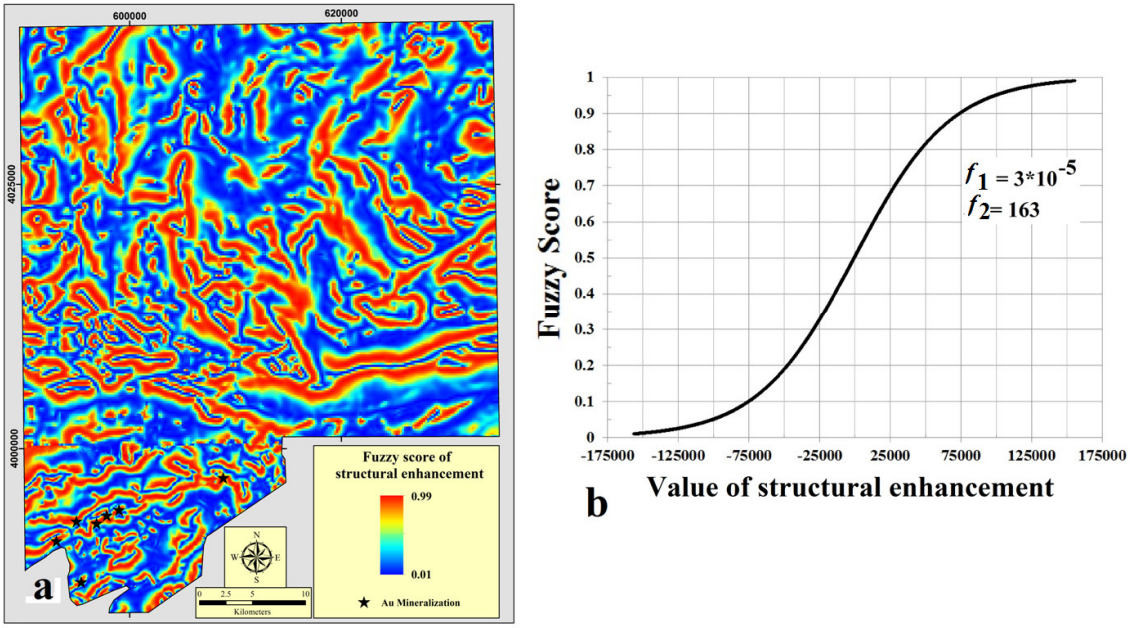

Fig. 4. Fuzzy evidence layer of pathways (a) and variation of weights, assigned by large fuzzification function, versus corresponding original evidence values (b).

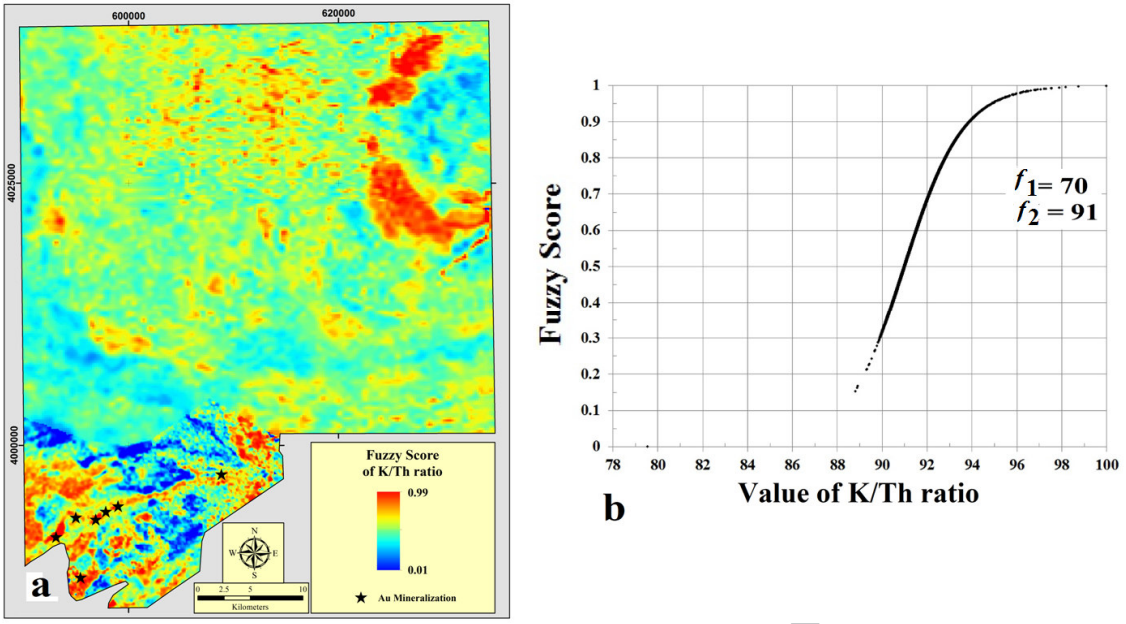

Fig. 5. Fuzzy evidence layer of hydrothermal activities (a) and variation of weights, assigned by large fuzzification function, versus corresponding original evidence values (b).

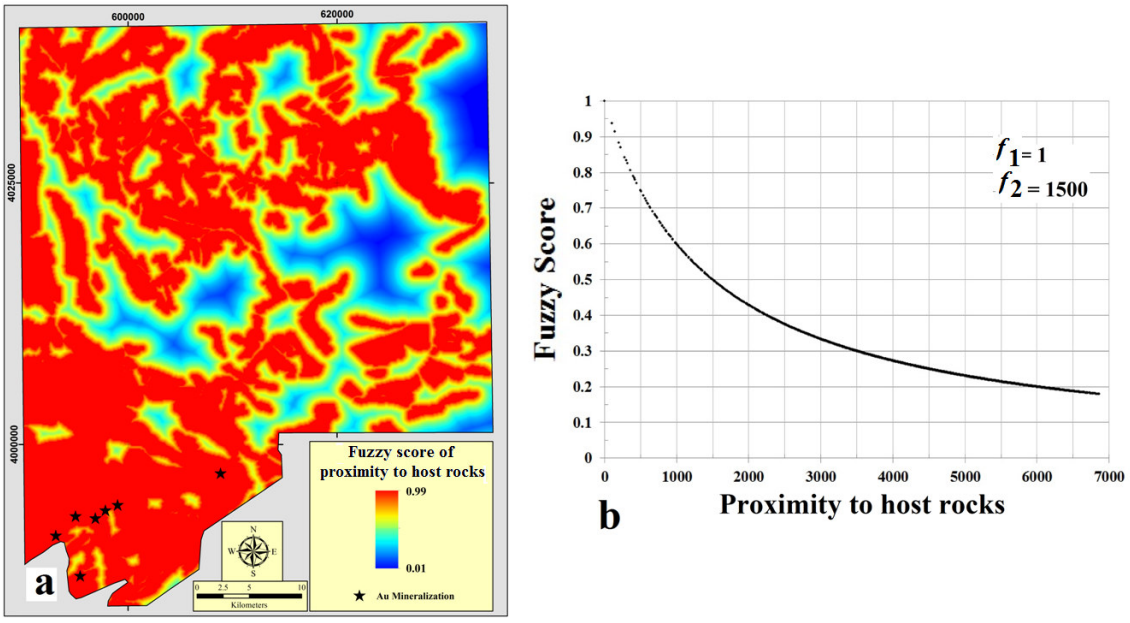

Fig. 6. Fuzzy evidence layer of ore raps (a) and variation of weights, assigned by small fuzzification function, versus corresponding original evidence values (b).

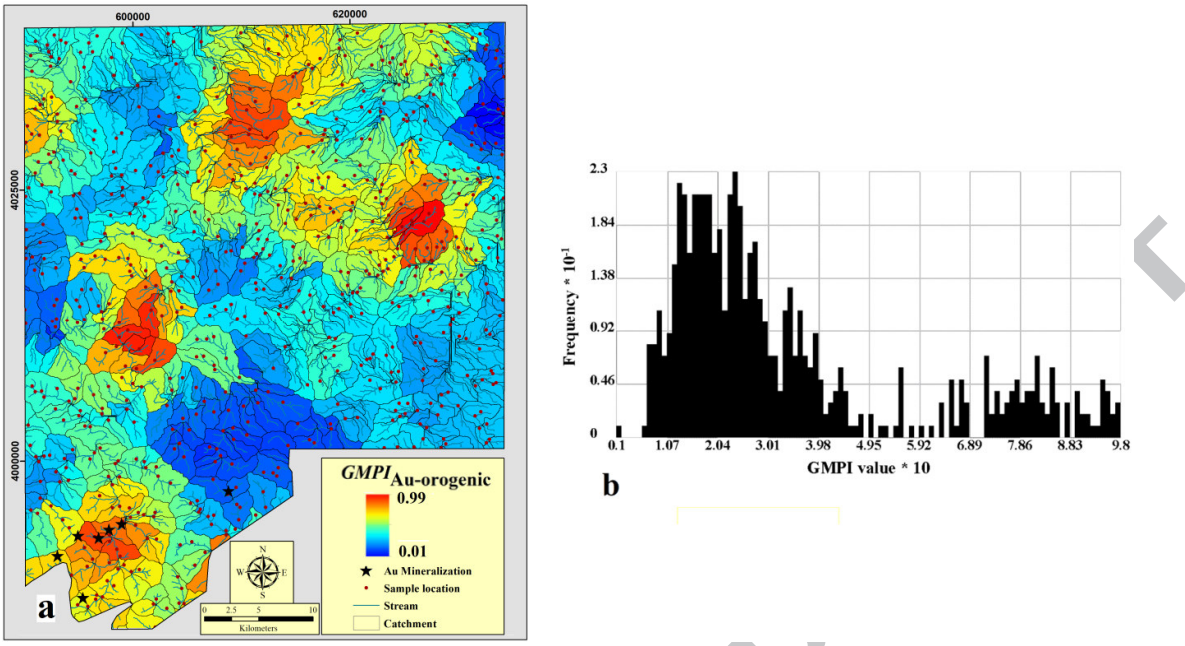

Fig. 7. Multi-element geochemical signature of orogenic gold deposition in the study area represented as geochemical mineralization prospectivity index, *GMPI* $_{Au\text{-}orogenic}$, fuzzified geochemical evidence layer (a) and histogram of the final GMPI values of orogenic gold deposits. The histogram of the final GMPI values shows two major populations meaning as Yousefi et al., (2012, 2014) demonstrated transformation of evidential values using logistic function facilitate recognition of geochemical patterns, anomalies, or populations.

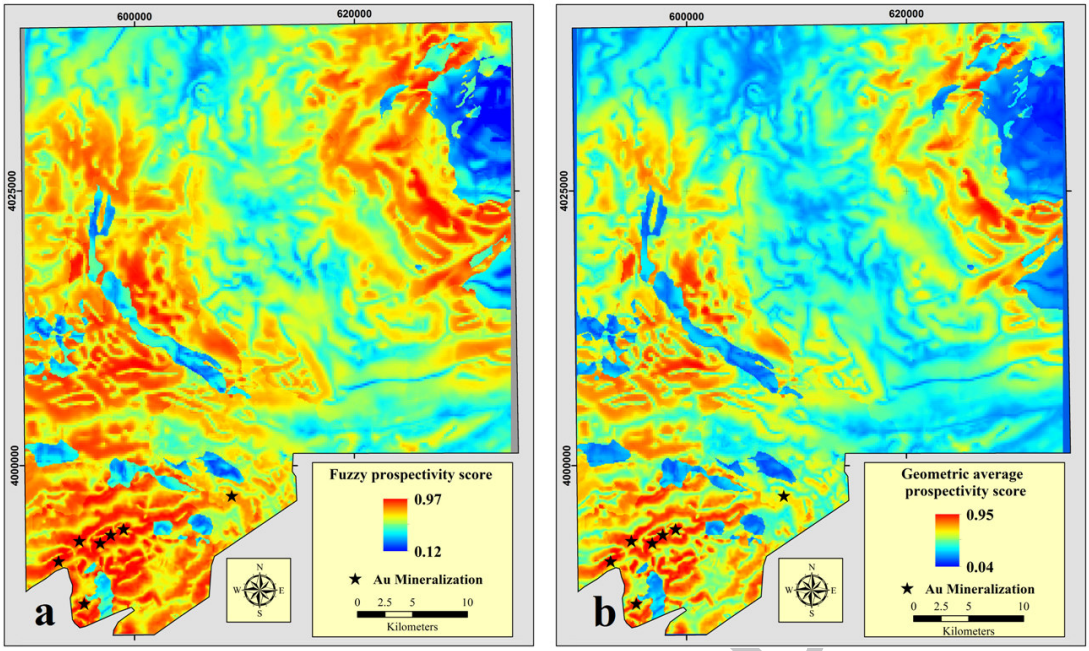

Fig. 8. Prospectivity model generated by fuzzy gamma (a) and geometric average (b) operators.

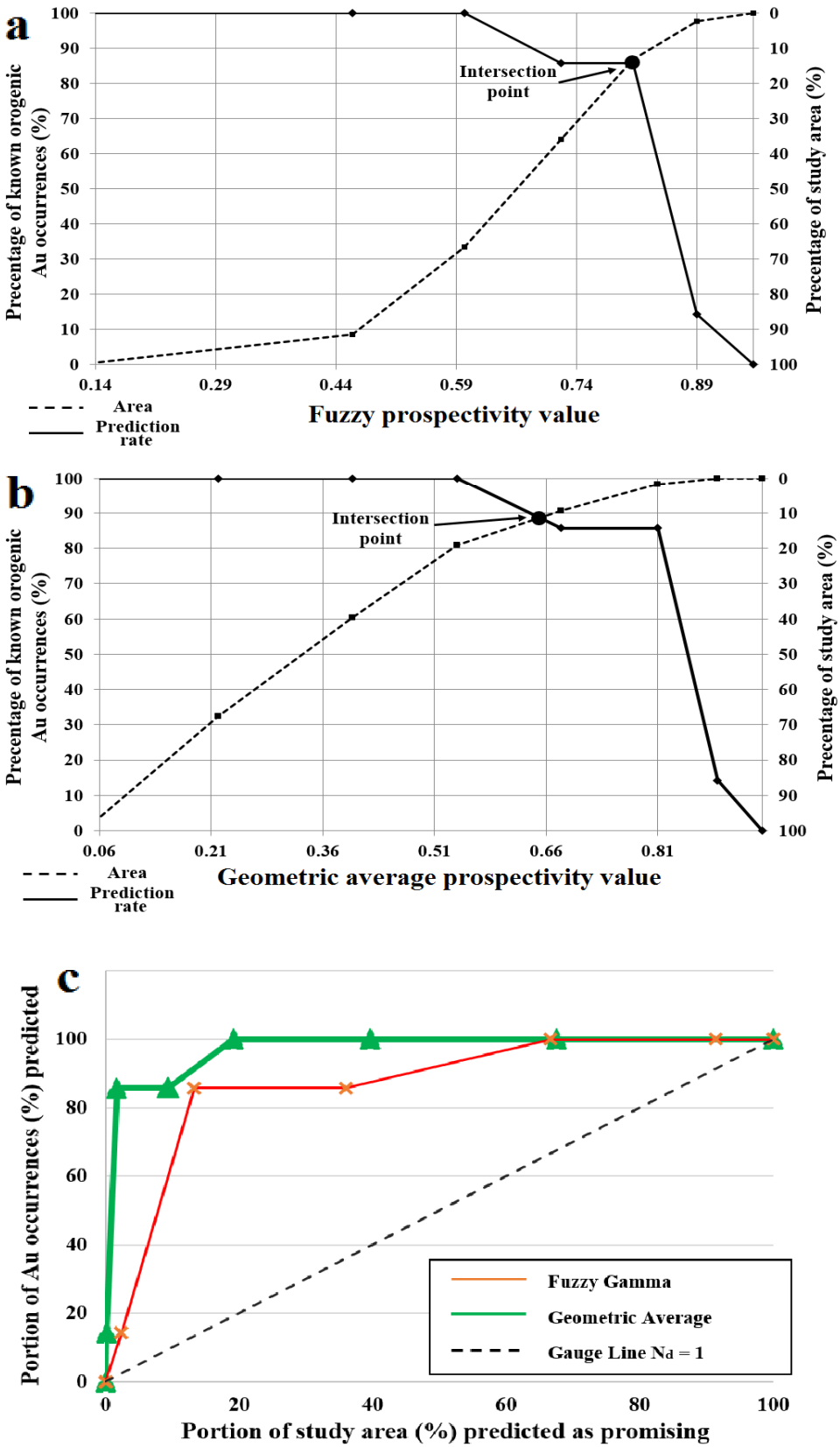

Fig. 9. Prediction-area plot of fuzzy (a) and geometric average (b) prospectivity models and success-rate curves of the two prospectivity models (c).

Table 1. Mineral system parameters (in general) of orogenic gold deposits

	Metal source	Thermal engine	Plumbing systems and pathways	Metal deposition	Physical ore traps
Exploration criteria	Mafic, ultramafic, and granitoids	Intrusive rocks	fault corridors, shear zones, and crustal discontinuities	complex polymetallic metal associations (e.g. Au ± Mo–W–Bi–Te–Cu-As-B-Sb-Te)	metagreywackes, metavolcanic, metasedimentary and totally metamorphic rock units
Translation to spatial proxy	1-Proximity to Mafic and ultramafic rocks 2-Proximity to granitoids	Proximity to Intrusive rocks	1- Proximity to faults 2-Fault density 3-Density of fault intersection 4-Density of lithological contact 5-Proximity to shear zones	Distribution maps of indicator elements (univariate and multivariate) in stream sediment, rocks and soil	1-Proximity to metavolcanics 2- Proximity to metasedimentary 3- Proximity to metamorphic rock 4- Proximity to granitoids

Table 2. Characteristics of gold deposits/occurrences in the study area

Deposit/ prospect	Lat / Long	Host rocks	Mineralization Style	Genetic type	Ore tonnage / Metal grade	Exploration stage	Data source
Qolqoleh	593094 / 3991293	Mafic to intermediate (andesite to andesitic basalt) meta-volcanic rocks and sericite schist	Sulfide (1-3%) bearing alteration zone, average 100m wide, 2400m long	Orogenic (ductile to brittle shear zone)	3 million tones / 3.5 g/t	Prospecting by trenches and drill holes	Aliyari et al. (2007, 2009), Tajeddin (2011)
Kervian	596877 / 3992948	Felsic to mafic meta-volcanic and metasedimentary rocks	Sulfide (1-5%) bearing alteration zone, average 100m wide, 2400m long	Orogenic (ductile to brittle shear zone)	1 million tones / 0.8 g/t	Prospecting by trenches and drill holes	Heidari (2004), Heidari et al. (2006), Aliyari et al. (2007, 2009), Tajeddin (2011)
Qabaqloujeh	599008 / 3994223	Meta-volcanic phyllite, schist and mylonitic	Sulfide (1-3%) bearing alteration zone, average 50m wide, 800m long	Orogenic (ductile to brittle shear zone)	2 million tones / 1 g/t	Prospecting by trenches and drill holes	Aliyari et al. (2007, 2009), Tajeddin (2011)
Hamzeh-Gharnein	594981 / 3993146	Chlorite schist mylonitic granites	Sulfide bearing alteration zone, average 60m wide, 700m long	Orogenic (ductile to brittle shear zone)	2.6 million tones / 1.35 g/t	Prospecting by trenches and drill holes	Tajeddin (2011)
Pir-Omran	595430 / 3987437	Meta- andesite, phyllite, schist & limestone	Quartz veins and veinlets, up to 3m wide, 200m long, with gold mineralization, rare sulfides	Orogenic (ductile to brittle shear zone)	Unstudied	Prospecting Old mining	Tajeddin (2011)
Kasnazan	608844 / 3997250	Meta-limestone mylonitic granites	Quartz veins and veinlets, up to 5m wide, 150m long, with sulfide & gold mineralization	Orogenic (ductile to brittle shear zone)	Unstudied	Prospecting	Tajeddin (2011)
Ghareh-Char	597838 / 3993710	Chlorite schist mylonitic granites	-	-	Unstudied	Prospecting by lithogeochemical samples	Tajeddin (2011)

- Geological processes of mineralization are translated to predictor maps
- Diverse spatial relationships between predictors and mineralization are investigated
- Different fuzzification functions are used to quantify the relationships